Rendiconti Lincei. Scienze Fisiche e Naturali (2024) 35:1–23
https://doi.org/10.1007/s12210-023-01217-6

CHEMICAL KINETICS AT MICRO-, MESO-, MACROSCALES

Crossed molecular beam studies of bimolecular reactions of atomic oxygen with nitrogen-bearing organic molecules (nitriles and N-heterocyclic)

Giacomo Pannacci[1] · **Gianmarco Vanuzzo**[1] · **Nadia Balucani**[1] · **Piergiorgio Casavecchia**[1]

Received: 23 October 2023 / Accepted: 15 December 2023 / Published online: 6 February 2024

Abstract
In this contribution, dedicated to the memory of Prof. Gian Gualberto Volpi, we provide a short review of recent work carried out in our laboratory on reactive scattering studies of the reaction dynamics of atomic oxygen with nitrogen-bearing organic molecules. Specifically, we focus on the polyatomic bimolecular reactions of atomic oxygen, both in the ground and first excited state, O(^{3}P) and O(^{1}D), with the simplest unsaturated nitriles, namely HCCCN (cyanoacetylene) and CH_2CHCN (cyanoethylene, or acrylonitrile), and with the simplest six-member ring N-heterocyclic compound, pyridine (C_5H_5N). Using the crossed molecular beam (CMB) scattering technique with *universal* electron-impact ionization mass-spectrometric detection and time-of-flight analysis to measure product angular and velocity distributions, the primary product channels and their branching fractions were determined, thus assessing the central role played by intersystem-crossing (ISC) in this class of reactions. The experimental work was synergistically accompanied by theoretical calculations of the relevant triplet and singlet potential energy surfaces (PESs) to assist the interpretation of experimental results and elucidate the reaction mechanism, including extent of ISC. Cyanoacetylene and cyanoethylene are of considerable interest in astrochemistry being ubiquitous (and relatively abundant) in space including comets and the upper atmosphere of Titan. Being oxygen the third most abundant element in space, the title reactions are of considerable relevance in the chemistry of extraterrestrial environments. In addition, they are also important in combustion chemistry, because thermal decomposition of pyrrolic and pyridinic structures present in bound N-containing fuels generates N-bearing compounds including, in particular, the above two nitriles.

Keywords Bimolecular reactions · Molecular beam reaction dynamics · O-atom reactions with N-bearing organic molecules · Combustion chemistry · Astrochemistry

1 Introduction

In 1968 *Gian Gualberto Volpi* (1928–2017, *Linceo* from 1994), together with collaborators Giorgio Liuti, Vincenzo Aquilanti, and Franco Vecchiocattivi, founded at the University of Perugia the research group "*Elementary Chemical Processes"* and began an exciting scientific journey that today still continues in Volpi's legacy (Boato and Volpi 1999). In 1990, within the various group activities that were inspired by Volpi with enthusiastic support and collaboration, we undertook a broad research program on the investigation of the dynamics of *elementary chemical reactions* by exploiting a newly built, advanced "*crossed molecular beam*" (CMB) instrument equipped with a rotatable quadrupole mass-spectrometer (MS) detector and a time-of-flight analysis system (Beneventi et al 1986a, b; Alagia et al. 1995; Casavecchia et al. 1999a, b; Casavecchia 2000). Establishing

This peer-reviewed research paper is part of the Topical Collection originated from contributions to the conference on "Chemical Kinetics at Micro-, Meso-, Bioscales", dedicated to Giangualberto Volpi (1928–2017, Linceo from 1994), organized by Accademia Nazionale dei Lincei and Fondazione Guido Donegani in Rome, March 27–28, 2023.

✉ Nadia Balucani
nadia.balucani@unipg.it

✉ Gianmarco Vanuzzo
gianmarco.vanuzzo@unipg.it

[1] Dipartimento di Chimica, Biologia e Biotecnologie, Università degli Studi di Perugia, 06123 Perugia, Italy

a research line on experimental *reaction dynamics* had been one of the main dreams of Volpi ever since he arrived in Perugia. The initial CMB instrument, built in the early 1980s and first employed for high-resolution elastic scattering experiments (Beneventi et al 1986a,b), was optimized for reactive scattering studies in 1990 (Balucani et al. 1991; Alagia et al. 1993a, b, 1995, 1996; Casavecchia et al. 1999a, b; Casavecchia 2000) and continuously updated over the years. In 2004, most notably, a major improvement, consisting in the implementation of *soft* ionization with tunable energy electrons for product detection (Capozza et al. 2004; Casavecchia et al. 2005; Balucani et al. 2006), permitted us to overcome the main limitation of the method until that time, namely, the problem of serious (elastic/inelastic) interferences in product detection due to dissociative ionization of products, reactants, and background gases, that made very difficult, and often impossible, to identify all the primary reaction products of multichannel bimolecular reactions. This problem had, in particular, severely hampered the application of the CMB-MS method to studies of bimolecular reactions exhibiting a variety of competing product channels, as are most reactions of atomic and molecular radicals with polyatomic molecules occurring in atmospheric, combustion, and astrochemical environments. Among these reactions, those of ground state atomic oxygen, $O(^3P)$, with unsaturated hydrocarbons are a most notable example. In fact, although the first kinetic investigation of the $O(^3P)$ reaction with the simplest alkene, ethylene, dates back to the mid-1950s (Cvetanović 1955), and various dynamical techniques, including the CMB method with *hard* (200 eV) electron ionization detection (Schmoltner et al. 1989) and various spectroscopic methods in pump-probe experiments (Endo et al. 1986) were subsequently applied in the following decades, it was not until 2004, with the implementation in the Perugia laboratory of *soft* electron ionization in CMB experiments with MS detection, that it became possible to probe, on the same footing, all competing product channels of multichannel bimolecular reactions, such as those of $O(^3P)$ with acetylene (Capozza et al. 2004) and ethylene (Casavecchia et al. 2005), and to derive the product branching fractions (BFs). The initial studies on $O(^3P)$ reactions with 2C unsaturated hydrocarbons (UHCs) (the simplest alkyne and alkene) were subsequently followed by studies involving 3C (alkyne, alkene, and diene) and 4C (alkenes and dienes, including conjugated dienes) UHCs, as well as the simplest aromatic hydrocarbons (benzene and toluene) (see further below).

From a more general perspective, we emphasize that during the 1990s in the field of reaction dynamics, after successful work in several laboratories on a series of 3-atom and 4-atom reactions of great fundamental interest, such as $H + D_2/HD$ (Schnieder et al. 1995; Yuan et al. 2018), $F + H_2/D_2/HD$ (Qiu et al. 2006; Chen et al. 2021), $Cl + H_2/D_2/HD$ (Alagia et al. 1996; Wang et al. 2008), $OH + D_2$ (Alagia et al. 1993a; Strazisar et al. 2000; Liu et al. 2012), and $OH + CO$ (Alagia et al. 1993b; Laganà et al. 2012), in which the experimental results were usually accompanied by detailed comparisons with the results of quasi-classical trajectory and/or accurate quantum scattering calculations on ab initio potential energy surfaces (PESs), the interest started to shift toward more complex (polyatomic) bimolecular reactions of importance also in areas of practical relevance, such as combustion and astrochemistry (including the atmosphere of Titan). These reactions involved mostly, among others, not only O, C, and N atoms (Casavecchia et al. 1999a, b; Leonori et al. 2008; Balucani et al. 2009) [which are the 3rd, 4th, and 5th most abundant elements in the interstellar medium (ISM)], but also S atoms (Leonori et al. 2009) and CN (Leonori et al. 2010) and OH radicals (Laganà et al. 2012; Liang et al. 2023a).

To improve current kinetic models of the above important environments, detailed information on the involved key elementary, neutral–neutral reactions is required. In particular, knowledge of the identity of the primary reaction products and their BFs is central. A most useful and powerful approach to elucidate the complex mechanisms of multichannel bimolecular reactions is to study them using a synergistic experimental and theoretical approach that can allow us to identify unambiguously all the primary reaction products, determine their BFs, and elucidate the overall reaction mechanism. This was achieved by combining CMB-MS experiments and high-level theoretical calculations of the underlying PESs, as well as dynamical and/or statistical calculations on these PESs of the product BFs as a function of energy (temperature) (Leonori et al. 2015; Caracciolo et al. 2019a; Cavallotti et al. 2022). For $O(^3P)$ reactions, pronounced intersystem crossing (ISC) effects were observed in most systems. We remind that the quantum effect of ISC, formally forbidden within the nonrelativistic quantum theory, derives from the fact that the first excited state of the oxygen atom is a ^1D state that correlates with a singlet PES. The latter starts higher in energy and goes much lower than the triplet one. So, a crossing between the two PESs occurs and a transition from the triplet to the singlet PES is possible, enhancing the number of possible products by opening up new reaction channels. ISC effects for 3C- and 4C-UHCs and aromatics were theoretically elucidated using coupled triplet-singlet PESs and statistical Rice-Ramsperger-Kassel-Marcus/Master Equation (RRKM/ME) calculations of product BFs, with inclusion of ISC effects, in collaboration with Carlo Cavallotti (Politecnico of Milan). For some of these reactions, once the theoretical results were found validated by a satisfactory comparison with experimental results in CMB conditions, the theoretical approach was exploited to

predict product BFs and, often, also channel-specific rate constants as a function of temperature (Leonori et al. 2015; Caracciolo et al. 2019a; Cavallotti et al. 2022), which is the needed information for improving current kinetic models of combustion as well as of astrochemical environments. Critical in most of our studies on multichannel bimolecular reactions has been the use of *soft* electron-ionization detection (Casavecchia et al. 2009; Caracciolo et al. 2019a). In other laboratories, *soft* photo-ionization detection exploiting tunable vacuum-ultra-violet (VUV) synchrotron radiation was used both in pulsed CMB-MS experiments (Lee et al. 2009) and in kinetic experiments (Taatjes et al. 2008; Osborn et al. 2008).

Over the past 20 years or so, we have been using the above strategy of coupling synergistically experiment and theory, initially in collaborations with Joel Bowman (Emory University) for $O(^3P) + C_2H_4$ (Fu et al. 2012a, b; Balucani et al. 2015a) and later on, for more complex reactions, with Carlo Cavallotti (Politecnico of Milan), Marzio Rosi (University of Perugia), and Dimitrios Skouteris (Master-Up, Perugia), to investigate a variety of bimolecular reactions of relevance in combustion chemistry, astrochemistry, and the atmosphere of Titan, such as:

(i) Reactions of ground state atomic oxygen, $O(^3P)$ (also excited $O(^1D)$ in some cases) with unsaturated aliphatic [acetylene (Leonori et al. 2014), ethylene (Fu et al. 2012a, b; Balucani et al. 2015a), allene (Leonori et al. 2012a), propene (Cavallotti et al. 2014; Leonori et al. 2015), propyne (Vanuzzo et al. 2016a, b; Gimondi et al. 2016), 1-butene (Caracciolo et al. 2019a), 1,2-butadiene (Caracciolo et al. 2019b), 1, 3-butadiene (Cavallotti et al. 2022)], and aromatic hydrocarbons [benzene (Cavallotti et al. 2020; Vanuzzo et al. 2021), toluene (Balucani et al. 2024)], the prototype N-heterocyclic, pyridine (Recio et al. 2022), and ubiquitous nitriles [cyanoacetylene (Liang et al. 2023b), cyanoethylene (Pannacci et al. 2023)].

(ii) Reactions of excited atomic nitrogen, $N(^2D)$, with saturated [methane (Balucani et al. 2009), ethane (Balucani et al. 2010)] and unsaturated hydrocarbons [acetylene (Balucani et al. 2000), ethylene (Balucani et al. 2012), propyne (Mancini et al. 2021), allene (Vanuzzo et al. 2022b)], with aromatic hydrocarbons [benzene (Balucani et al. 2023), toluene (Vanuzzo et al. 2024)], pyridine (Recio et al. 2021), cyanoacetylene (Liang et al. 2022), and cyanoethylene (Vanuzzo et al. 2022a).

(iii) Reactions of carbon atoms, $C(^3P)$, and CN radicals with unsaturated hydrocarbons [acetylene (Casavecchia et al. 2001; Leonori et al. 2008, 2010), ethylene (Geppert et al. 2003; Leonori et al. 2012b; Balucani et al. 2015b)]; of $S(^1D)$ with saturated (CH_4) and unsaturated hydrocarbons (C_2H_2, C_2H_4) (Leonori et al. 2009; Berteloite et al. 2011), and of CN with also nitriles [cyanoacetylene (de Aragão et al. 2024), cyanoethylene (Marchione et al. 2022)].

In this contribution, we provide a short review of some of the most interesting results very recently obtained in our laboratory on the dynamics of the multichannel reactions of $O(^3P)$ with N-bearing unsaturated hydrocarbons, specifically, the simplest unsaturated nitriles, cyanoacetylene and cyanoethylene (acrylonitrile), and with the simplest 6-member ring, N-heterocyclic molecule, namely, pyridine. As already noted, these systems are of relevance in areas ranging from combustion to astrochemistry, including biology and astrobiology.

2 Experimental method

The basic methodology of crossed molecular beam reactive scattering with mass spectrometric detection is well established (Lee 1987a, b; Herschbach 1987; Casavecchia 2000). The CMB-MS technique is arguably the most powerful experimental method for studying the dynamics of bimolecular reactions at the microscopic level. In fact, MS, either by electron-impact ionization or photo-ionization, is a *universal* detection method. This is particularly advantageous, actually crucial when studying polyatomic multichannel reactions, because the different products can be probed on the same footing, while this is not possible, for instance, using laser spectroscopy methods. Critical in MS product detection for multichannel reactions is the use of *soft* ionization, either using tunable low energy electrons (Casavecchia et al. 2005, 2009, 2015) or tunable VUV photons, as can be afforded by third generation synchrotrons (Yang et al. 1997; Lee et al. 2009) or even table-top lasers [in this case the selection of photon energies is limited, but the approach still remains powerful in many cases (Albert and Davis 2013)]. The great advantage of soft ionization in CMB-MS experiments is the gained capability of limiting or, often, even suppressing completely the problem of dissociative ionization of reactants, products, and background gases.

A description of our CMB apparatus, including the implementation of *soft* electron ionization, has been provided in previous articles and reviews. (Alagia et al. 1995; Casavecchia 2000; Casavecchia et al. 2009, 2010; Caracciolo et al. 2019c). We wish to emphasize that, because absolute electron-ionization (EI) cross sections are usually known or can be reliably estimated for most species, once measured in the

laboratory (LAB) the product angular and velocity distributions of the various competing product channels, the use of *soft* EI allows us to derive the product branching fractions from the observed product number densities and velocities and their conversions into product angular and translational energy distributions in the center-of-mass (CM) reference frame (Casavecchia et al. 2009, 2015).

A most recent technical improvement of our apparatus has seen the replacement of two freon-baffled diffusion pumps (effective pumping speed of 1200 and 1600 l/s) and an old cryopump (3500 l/s, 20 K), used to pump the main, large scattering chamber, with two magnetically suspended turbomolecular pumps (pumping speed 1850 l/s each) backed by a large dry roots pump (110 m^3/h) and a new cryopump (3600 l/s, 10 K) (Murray et al. 2020) Although the ultimate vacuum of the main chamber is only slightly improved (by more than a factor of two), the new pumping speed is overall higher and the vacuum cleaner, which reduces the main chamber effusion in the ultra-high-vacuum (UHV) detector (kept below 1×10^{-10} mbar by extensive turbo- and cryo-pumping).

In our CMB apparatus, two supersonic beams of atomic and molecular species are produced with narrow angular and velocity spread and made to cross in a high-vacuum chamber (maintained in the 10^{-7} mbar ($= 10^{-5}$ Pa) pressure range in operating conditions), typically at 90°, but also 45° or 135° are uniquely possible for reaching lower and higher, respectively, collisions energies while maintaining the same beam characteristics (Balucani et al. 2006; Leonori et al. 2008). Product angular distributions, $N(\Theta)$, are measured by modulating the molecular beam at 160 Hz for background subtraction. When measuring TOF distributions, $N(\Theta,t)$, a chopper wheel is placed in front of the detector, which is composed of a tuneable electron-impact ionizer followed by a quadrupole mass filter and a Daly type ion detector (Daly 1960). Single-shot TOF is used for beam characterization, while the higher duty-cycle pseudo-random chopping method is used for measuring the product TOF distributions. The ionizer is located in the innermost region of the triply differentially pumped UHV detector chamber. The detector chamber can be rotated in the collision plane, around the axis orthogonal to the plane of the two beams passing through the collision center.

The product $N(\Theta)$ and $N(\Theta,t)$ distributions are measured in the LAB reference frame, but for the physical interpretation of the scattering results a coordinate transformation from the LAB to the center-of-mass (CM) reference frame is required (Lee 1987b). For each reaction channel the relation between LAB and CM product flux is given by $I_{LAB}(\Theta,v) = I_{CM}(\theta,u)v^2/u^2$, where Θ and v are the LAB scattering angle and velocity, respectively, while θ and u are the corresponding CM quantities. Since the EI mass-spectrometer detector measures the product number density, $N_{LAB}(\Theta,v)$, rather than the flux, $I_{LAB}(\Theta,v)$, the actual relation between the LAB density and the CM flux is given by $N_{LAB}(\Theta) = I_{CM}(\theta,u)v/u^2$. Analysis of the LAB data is performed by forward convolution of trial CM distributions over the experimental conditions (beam divergences in angle and velocity, and detector angular resolution). The CM reactive differential cross section $I_{CM}(\theta,u)$ is commonly factorized into the product of the velocity (or translational energy) distribution, P(u) [or $P(E'_T)$], and the angular distribution, $T(\theta)$: $I_{CM}(\theta, E) = T(\theta) \times P(E'_T)$. In some cases the coupling between the $T(\theta)$ and $P(E'_T)$ functions needs to be accounted for. The $T(\theta)$ and $P(E'_T)$ functions contain all the information about the reaction dynamics. When multiple reaction channels contribute to the signal at a given mass-to-charge (*m/z*) ratio, as in the reaction systems discussed here, a more complex situation arises. In these cases a weighted total CM differential cross section reflecting the possible contributions for a specific *m/z* value is used in the data analysis of the LAB distributions, that is, $I_{CM}(\theta,E'_T) = \sum_i w_i \times [T(\theta) \times P(E'_T)]_i$, with the parameter w_i representing the relative contribution of the integral cross section of the ith channel (Casavecchia et al. 2009, 2015). The $T(\theta)$ and $P(E'_T)$ functions and the relative weight w_i for each channel are iteratively adjusted until calculated LAB angular distributions and TOF spectra reproduce the experimental ones. Once the $T(\theta)$ and $P(E'_T)$ functions for the various product channels are characterized, the branching fraction of each primary product can be estimated by using the procedure introduced by Schmoltner et al. (1989) and widely employed by us in the study of a variety of multichannel reactions of $O(^3P)$ with UHCs (Casavecchia et al. 2015; Caracciolo et al. 2019a; Vanuzzo et al. 2021).

2.1 The reactions of $O(^3P,^1D)$ with unsaturated nitriles

The simplest unsaturated nitriles, cyanoacetylene (HC_3N) and cyanoethylene (acrylonitrile) (C_2H_3CN), are particularly important in combustion chemistry and astrochemistry. The inclusion of the oxidation processes of cyanoacetylene and acrylonitrile in models that simulate the combustion of coals and other low-rank fossil fuels is important to account for dangerous emissions. This because the nitrogen content of many fuels is essentially ascribed to the presence of pyrrolic and pyridinic structures (Snyder 1969; Brandenburg and Latham 1968; Wallace et al. 1989), but their thermal decomposition generates many nitrogen-bearing compounds, including cyanoacetylene and acrylonitrile (Mackie et al.

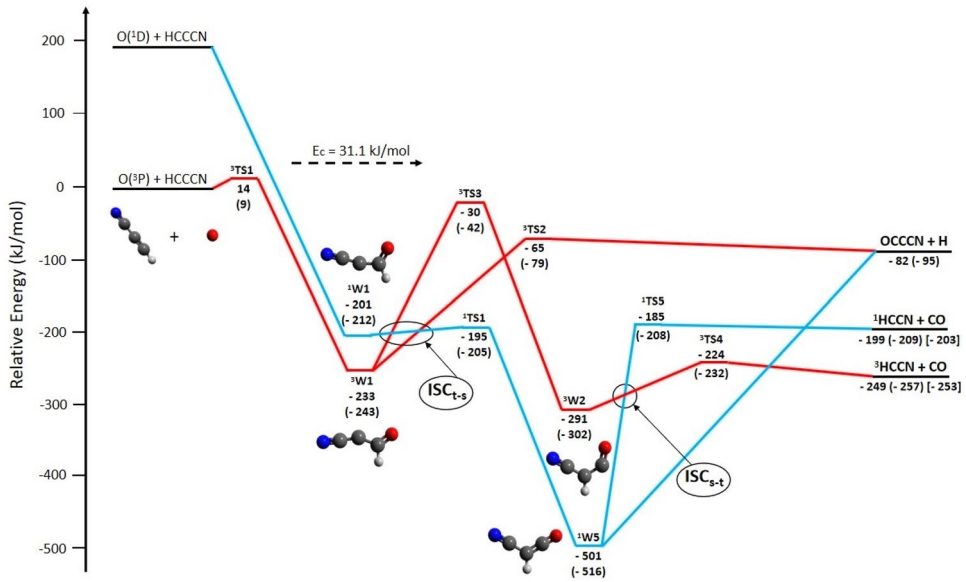

Fig. 1 Schematic, simplified (see text) triplet (red lines) and singlet (blue lines) potential energy surfaces for the $O(^3P,^1D)+HC_3N$ reactions calculated at the CCSD(T)/aug-cc-pVTZ//B3LYP/aug-cc-pVTZ level of theory (adapted from Liang et al. 2023b). The reaction pathways explored by the reactive flux are indicated in bold red and blue solid lines on triplet and singlet PES, respectively; they are the channels 1, 2, and 4; channel (3) leading to $^3CCO+HCN$ products, although more exothermic than channels (4) is not reported due to the presence of an interconversion barrier so high that the BF is negligible (see Liang et al. 2023b). The intersystem crossing (ISC) region where the surface-hopping from the triplet to the singlet PES (ISC_{t-s}) in the entrance channel is more likely to occur, is indicated with an ellipse. Indicated with a circle is also the possible singlet-to-triplet crossing in the exit channel (ISC_{s-t}), which has been assumed to be negligible (adapted from Liang et al. 2023b) (color figure online)

1990; Lifshitz et al. 1989; Hore and Russell 1998; Terentis et al. 1992), that can undergo subsequent oxidation to NO_x (Finlayson-Pitts and Pitts 1986). For the above reasons, it is worth investigating the reactions of cyanoacetylene and acrylonitrile with common oxidant species in combustion, including atomic oxygen. Information on the primary products and branching fractions for the reactions $O(^3P)+HC_3N$ and $O(^3P)+C_2H_3CN$ are expected to be useful for improving combustion models.

In addition, the $O(^3P)$ + cyanoacetylene and $O(^3P)$ + acrylonitrile reactions are also relevant in the chemistry of the interstellar medium, being these two nitriles ubiquitous in space. In fact, HC_3N was first detected in 1971 in the galactic star-forming region Sgr B2 (Turner 1971) and has since been observed in a variety of interstellar environments, including molecular clouds, solar-type protostars, circumstellar envelopes and external galaxies (Turner 1971; Walmsley et al. 1986; van Dishoeck et al. 1995; Jaber Al-Edhari et al. 2017; Suzuki et al. 1992; Aladro et al. 2011, 2015; Lindberg et al. 2011; Costagliola et al. 2011). HC_3N is also one of the few molecules observed in protoplanetary disks (Chapillon et al. 2012) and it has been detected in cometary comas (Bockelée-Morvan et al. 2000; Hänni et al. 2021; Biver et al. 2015) as well as in the upper atmosphere of Titan, the massive moon of Saturn (Teanby et al. 2007). In addition to being ubiquitous, interstellar HC_3N has a relatively large abundance with respect to H_2 (which is, by far, the most abundant molecule in space). Regarding acrylonitrile, it is the first molecule with a C=C double bond detected in the ISM (Ceccarelli et al. 2017; McGuire 2022). After the first detection in Sagittarius (Sgr) B2 (Ceccarelli et al. 2017), acrylonitrile has been identified in a variety of interstellar environments, such as the hot molecular core Sgr B2(N) (Turner 1971; Walmsley et al. 1986), Orion-KL (van Dishoeck et al. 1995), the TMC-1 dark cloud (Jaber Al-Edhari et al. 2017), the circumstellar envelope of the C-rich star IRC + 10216 (Jaber Al-Edhari et al. 2017), and the L1544 prototypical prestellar core (Aladro et al. 2011), as well as in Titan's atmosphere (Lindberg et al. 2011; Aladro et al. 2015; Costagliola et al. 2011; Chapillon et al. 2012; Bockelée-Morvan et al. 2000; Hänni et al. 2021; Biver et al. 2015). Being $O(^3P)$ quite abundant in various regions of the ISM, its reactions with the above two nitriles might contribute to control the abundance of HCCCN and CH_2CHCN in various extraterrestrial environments, and should be included in astrochemical models, where instead, so far, these reactions have been overlooked.

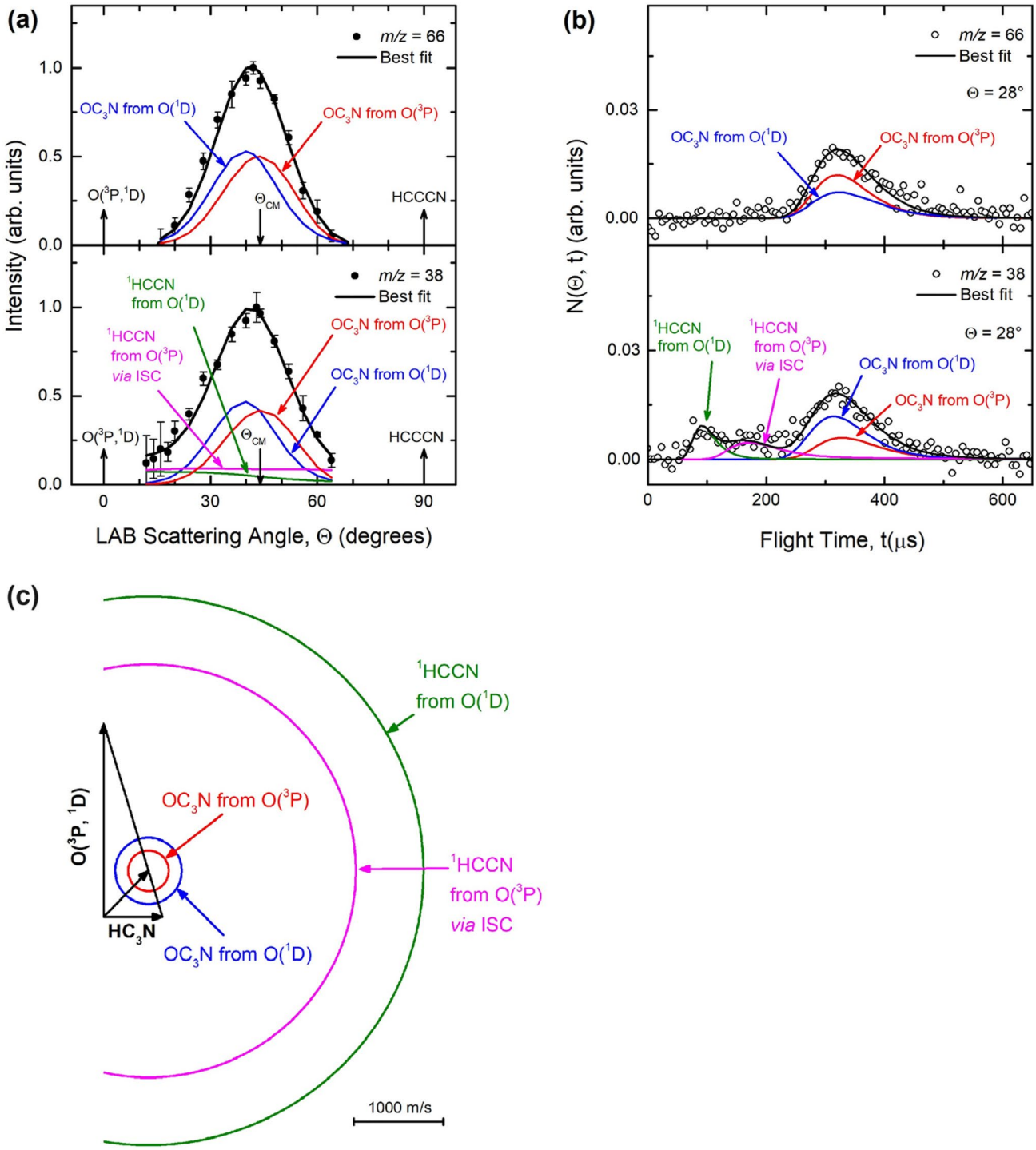

It should be noted that also atomic oxygen in its first excited state, O(^{1}D), can have an important role in governing the chemistry of several extraterrestrial environments, being its reactions called into play to elucidate the formation routes of complex organic molecules in cometary comas (Teanby et al. 2007) and interstellar ice (Mumma and Charnley 2011). Therefore, the study of the reaction of cyanoacetylene and acrylonitrile with also O(^{1}D) can contribute to enrich current astrochemical models.

The goal of our study on the reactions of O(^{3}P) with HC_3N and C_2H_3CN was to provide useful information on the nature of the primary products and their BFs for inclusion in improved astrochemical and combustion models.

◂**Fig. 2** **a** LAB angular distributions, N(Θ), measured at *m/z* = 66 (top panel) and *m/z* = 38 (bottom panel) for the $O(^3P,^1D)+HC_3N$ reactions at E_c = 31.1 kJ/mol. The black curves represent the calculated total angular distribution, N(Θ), when the weighted best-fit CM functions of Fig. 3 are used for the $O(^3P)$ and $O(^1D)$ contributions to the OC_3N product (top panel) and to the OC_3N and HCCN products (bottom panel). The relative contributions from $O(^3P)$ and $O(^1D)$ reactions to *m/z* = 66 and 38 are indicated and color coded. **b** Product LAB TOF distributions, N(Θ,t), measured at *m/z* = 66 (top panel) and *m/z* = 38 (bottom panel) at the LAB angle Θ = 28° for the reactions $O(^3P,^1D)+HC_3N$ at E_c = 31.1 kJ/mol. Open circles: experimental data. Black curves: calculated total TOF distributions when using the weighted best-fit CM functions of Fig. 3 for the $O(^3P)$ and $O(^1D)$ contributions to OC_3N and HCCN formation, respectively. The distinct contributions from $O(^3P)$ and $O(^1D)$ reactions to the calculated total TOF distributions are also indicated (line and color notations as in **a**). **c** Newton (velocity vector) diagram of the experiment. Here the various circles delimit the maximum speed that the indicated products from the $O(^3P,^1D)+HC_3N$ reactions at E_c = 31.1 kJ/mol can attain if all the available energy is channeled into product translational energy. Red line: Newton circles for the H-displacement channel leading to OC_3N from the $O(^3P)$ reaction. Blue line: same for the $O(^1D)$ reaction. Magenta line: Newton circle for the ^{1}HCCN product from the $O(^3P)$ reaction (via ISC). Violet line: Newton circle for the ^{3}HCCN product from the adiabatic $O(^3P)$ reaction. Green line: Newton circle for the ^{1}HCCN product from the adiabatic $O(^1D)$ reaction (adapted from Liang et al. 2023b) (color figure online)

We add that, recently, we have investigated the reactions of the above two nitriles not only with atomic oxygen, but also with other radicals that are abundant in extraterrestrial environments where HC_3N and C_2H_3CN have been identified, such as $N(^2D)$ (Liang et al. 2022) (Titan and comets) and CN (de Aragão et al. 2020, 2021, 2022) (Titan, interstellar clouds, and comets).

Below, we summarize the main results obtained from our recent CMB and theoretical studies on the dynamics and mechanism of these two reactions.

2.2 $O(^3P,^1D)+HCCCN$ (cyanoacetylene)

Despite the relevance of the $O(^3P)+HC_3N$ reaction in both astrophysical and combustion environments, there were very few experimental/theoretical studies on this reaction prior to our recent study (Liang et al. 2023b).

According to electronic structure calculations of the relevant triplet and singlet PESs from our recent work (Liang et al. 2023b), and also from previous, less detailed work (Xie et al. 2006), for the $O(^3P)+HC_3N$ reaction there are five possible exothermic channels, one nearly thermoneutral, while several others are substantially endothermic. The most exothermic ones, which include the product channels (in bold) found to be dominant in our study, are the following:

$O(^3P)+HCCCN$

→ ^{3}HCCN + CO ΔH°_0 = −249(−257) [−253] kJ/mol (1a)

→ **^{1}HCCN + CO ΔH°_0 = −199 (−209) [−203] kJ/mol** (**2a**)

→ ^{3}CCO + HCN ΔH°_0 = −109(−115) [−112] kJ/mol (3a)

→ **OCCCN + H ΔH°_0 = −82 (−95) kJ/mol** (**4a**)

The indicated standard enthalpies of reaction at 0 K, ΔH°_0, are those calculated at the CCSD(T) level and CCSD(T)/CBS level (values in parenthesis) (Liang et al. 2023b). In square brackets are also the values from available enthalpies of formation at 0 K (Ruscic et al. 2004, 2005; Ruscic and Bross 2020).

Figure 1 shows a simplified scheme of the triplet (red lines) and singlet (blue lines) PESs for the reactions $O(^3P,^1D)+HC_3N$, with only the main product channels depicted. In the figure, ISC regions between the triplet and singlet PES are indicated with an ellipse in the entrance channel ($ISC_{t\text{-}s}$) and with a circle in the exit channel ($ISC_{s\text{-}t}$). For a more detailed PES portraying also the other energetically open channels (which, however, were not observed to occur), see Fig. 6 in ref. Liang et al. (2023b) and Fig. S1 in its Supporting Information.

The corresponding channels (1b)–(4b) for the $O(^1D)$ reaction are more exoergic by 190 kJ/mol (the ^{3}P-^{1}D energy separation), and therefore are all strongly exothermic:

$O(^1D)+HCCCN$

→ ^{3}HCCN + CO ΔH°_0 = −439(−447) [−443] kJ/mol (1b)

→ **^{1}HCCN + CO ΔH°_0 = −389 (−399) [−393] kJ/mol** (**2b**)

→ ^{3}CCO + HCN ΔH°_0 = −299(−305) [− 302] kJ/mol (3b)

→ **OCCCN + H ΔH°_0 = −272 (−285) kJ/mol** (**4b**)

While channel (2a) can only be formed via ISC from the triplet to the underlying singlet PES in the entrance channel of the reaction, channels (1a) and (3a) (not shown in Fig. 1) can occur only adiabatically on the triplet PES, and channel (4a) can occur on both the triplet and singlet PES. We have searched for all channels (1a–4a)/(1b–4b), but have observed reactive signal only attributable to channels (2a)/(2b), that is, formation of CO + ^{1}HCCN (cyanomethylene, also termed cyanocarbene) and channels (4a)/(4b), that is, formation of OCCCN (cyanoketyl) + H. We emphasize that channels a and b (from $O(^3P)$ and $O(^1D)$, respectively) can be differentiated because of their different thermochemistry (see below).

Reactive scattering signals were measured at *m/z* = 66 ($OCCCN^+$) and *m/z* = 38 (CCN^+). Because for *m/z* = 38 there were interferences from daughter ions of the HC_3N reactant elastically/inelastically scattered by the oxygen seeded beam, the use of *soft* ionization (28 eV electrons were sufficient) was crucial for obtaining reliable results on the product channels. Notably, the presence of some $O(^1D)$ in our atomic oxygen beam, which is mainly composed by $O(^3P)$ (about 90%) (Alagia et al. 1997), permitted us to obtain

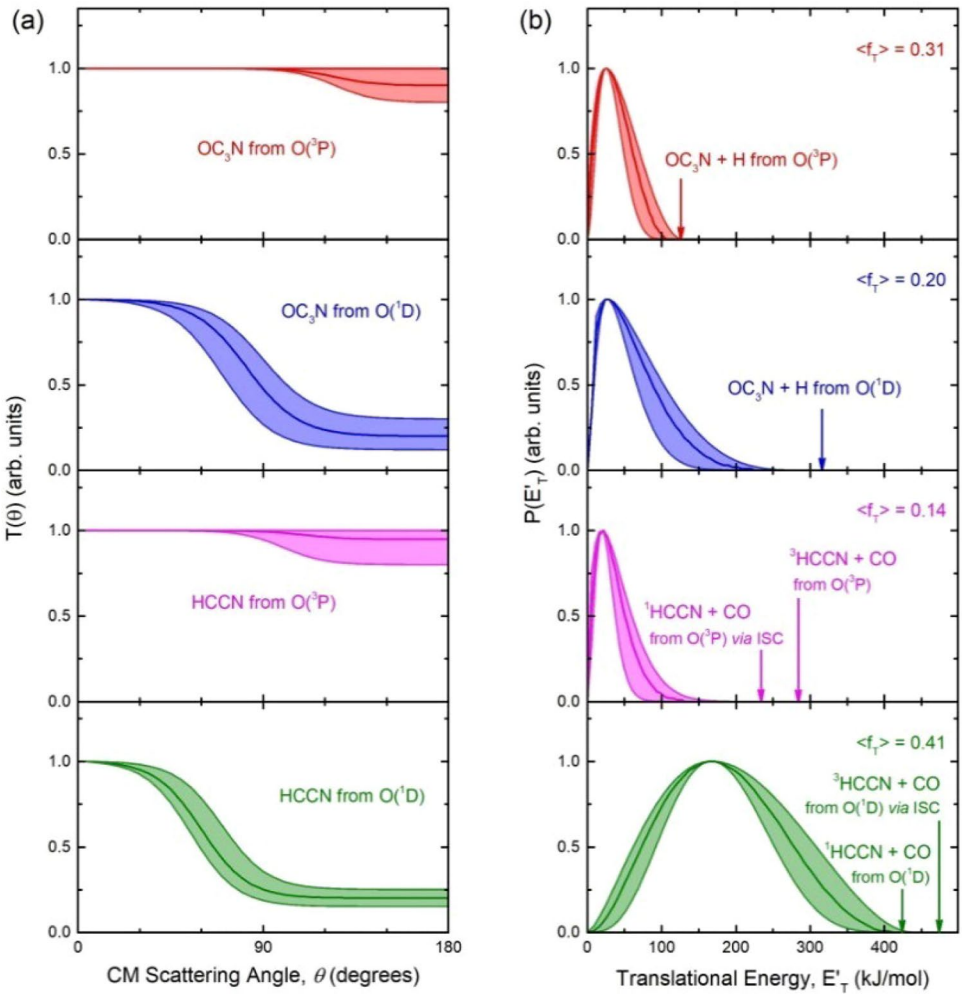

Fig. 3 Best-fit CM angular, T(θ) (left panels), and translational energy, $P(E'_T)$ (right panels), distributions for all (four) contributions used to reach the best-fit of the experimental data shown in Fig. 2a, b for the $O(^3P, ^1D) + HC_3N$ reactions at $E_c = 31.1$ kJ/mol. Line and color notations are as in Fig. 2. The shaded areas represent the error bars determined for the best-fit CM functions. Solid arrows in right-hand-side (*rhs*) panels indicate the total available energy ($E_{TOT} = \Delta H^0_0 - E_c$) for each specified product channel from the $O(^3P)$ and $O(^1D)$ reactions. The average fraction of the total available energy, for each channel, released as product translational energy, $\langle f_T \rangle$, is also indicated (from Liang et al. 2023b) (color figure online)

information on also the $O(^1D) + HC_3N$ reaction dynamics. In Fig. 2a, b we show product angular distributions measured at $m/z = 66$ (top panel) and $m/z = 38$ (bottom panel), and the TOF spectra at the same two masses (at the exemplary LAB angle $\Theta = 28°$), respectively. Figure 2c shows the velocity vector diagram of the experiment.

It should be noted that while $m/z = 66$ corresponds to the parent ion of the heavy coproduct, OC_3N, of channel (4a) and possibly also (4b), $m/z = 38$ (CCN^+) corresponds to the (− 1) daughter ion of the HCCN product from channels (1a)/(1b), (2a)/(2b), and possibly also to the (− 28) daughter ion of the OC_3N product from channels (4a)/(4b). HCCN products were detected at the (− 1) daughter ion $m/z = 38$ rather than at the parent ion mass of 39 for signal-to-noise reasons. The $m/z = 66$ LAB angular distribution shown in Fig. 2a (top panel) corresponding to the heavy coproduct OC_3N of the H-displacement channels (4a)/(4b) is peaked around the CM angle ($\Theta_{CM} = 44.1°$) and is quite narrow being confined within a small Newton circle (Fig. 2c). The single peak structure in the TOF spectrum (peaked around 300 μs) (Fig. 2b, top panel) is what is expected for the heavy coproduct of the possible H-displacement channels (4a)/(4b). The contribution of OC_3N from channels (4a)/(4b) is also visible at $m/z = 38$, through its daughter ion C_2N^+, in the recorded LAB distributions (see Fig. 2a, bottom panel) and especially in the TOF spectra (Fig. 2b, bottom panel). In order to fit the data at $m/z = 66$ it was necessary to use two sets of CM functions. These are shown in Fig. 3 (top two panels), and they were associated to the H-displacement channels (4a), leading to OC_3N from $O(^3P)$ on the triplet PES, and (4b),

Table 1 Product branching fractions (BFs) for the distinct $O(^3P) + HCCCN$ and $O(^1D) + HCCCN$ reactions (at $E_c = 31.1$ kJ/mol) (from Liang et al. 2023b)

Reactants	Products	PES involved	Experimental BF
$O(^3P) + HCCCN$	$^1HCCN + CO$	Singlet via ISC	0.90 ± 0.05
	$OC_3N + H$	Triplet	0.10 ± 0.05
$O(^1D) + HCCCN$	$^1HCCN + CO$	Singlet	0.94 ± 0.03
	$OC_3N + H$	Singlet	0.06 ± 0.03

The experimental uncertainties, ranging from 30 to 50%, are indicated

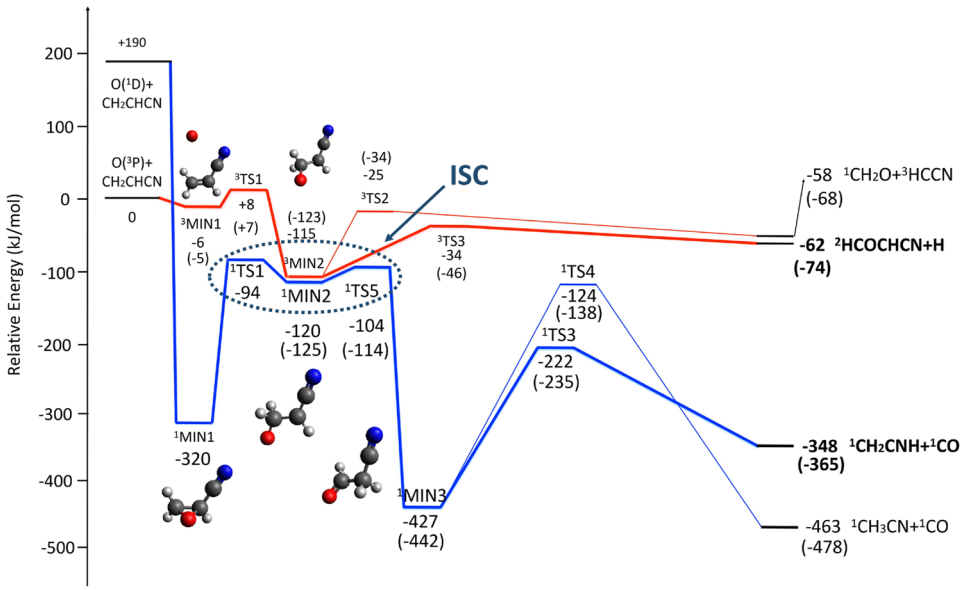

Fig. 4 Schematic representation of the simplified triplet (in red) and singlet (in blue) potential energy surfaces for the $O(^3P,^1D)+$acrylonitrile reactions with energy evaluated at the CCSD(T)/aug-cc-pVTZ level of theory and at the CCSD(T)/CBS level of theory (data in parentheses) for the most relevant channels (see text). In both cases the zero of the energy is represented by the $O(^3P)+CH_2CHCN$ reactants. The pathways leading to the two observed, most important channels (one reached adiabatically on the triplet and the other reached via ISC on the singlet PES) for the $O(^3P)+CH_2CHCN$ reaction are shown with thicker lines, together with a possible identification of the region of ISC (black dotted ellipse). For the more detailed PESs, see Pannacci et al. (2023) (adapted from Pannacci et al. 2023) (color figure online)

leading to OC_3N from $O(^1D)$ on the singlet PES. A possible small contribution of OC_3N from $O(^3P)$ via ISC was difficult to evaluate, but it is expected to be small. As can be seen from Fig. 2a (bottom panel) the $m/z=38$ LAB angular distribution is characterized by the same prominent peak centered around Θ_{CM} of the $m/z=66$ distribution (top panel), but it is clear that the $m/z=38$ distribution is not confined between 18° and 68° as the $m/z=66$ distribution, exhibiting significant additional intensity in the two wings. This is confirmed clearly by the TOF spectra at $m/z=38$ (Fig. 2b, bottom panel), where it is evident that, in addition to the pronounced peak centered at *ca.* 300 μs due to the fragmentation of the OC_3N product in the ionizer, there are also two distinct fast peaks, with the fastest one located at *ca.* 90 μs and the other at *ca.* 180 μs. The wings of the $m/z=38$ angular distribution and the two fast peaks in the $m/z=38$ TOF spectra could only be fitted by invoking two additional (with respect to the $m/z=66$ data) reactive contributions that, on the basis of energy and linear momentum conservation, can be unambiguously attributed to the HCCN products from the (1a)/(1b) and (2a)/(2b) channels.

From the shape of the CM angular distributions of Fig. 3 we can infer that formation of OC_3N and of HCCN from $O(^3P)$ proceeds via a *long-lived complex* mechanism (Levine and Bernstein 1987), while via a strongly *osculating complex* mechanism from $O(^1D)$, which reflects a substantially shorter intermediate complex lifetime in the case of the strongly exothermic $O(^1D)$ reactions.

The interpretation of the experimental results was assisted by dedicated electronic calculations of the triplet/singlet HC_3ON PESs (see Fig. 1) and statistical RRKM/ME calculations of product BFs, carried out separately on the adiabatic triplet and adiabatic singlet PESs (Liang et al. 2023b).

It was found that the $O(^3P)$ reaction dynamics with HC_3N is dominated by ISC from the entrance triplet PES to the underlying singlet PES (see Fig. 1), leading to the spin-forbidden $^1HCCN+CO$ product channel, with an estimated $BF=0.90\pm0.05$, while the H-displacement channel, formed adiabatically on the triplet PES, is minor, yet substantial, with $BF=0.10\pm0.05$. The experimentally derived BFs are summarized in Table 1 for both $O(^3P)$ and $O(^1D)$ reactions. This conclusion for the $O(^3P)$ reaction was derived from the observation that adiabatic theoretical calculations predict 98% of H channel on the triplet PES and 99% of CO channel on the singlet PES (see Table 2 in Liang et al. 2023b), which leads to a theoretical BF of 89% and 11% for the CO and H channels from $O(^3P)$, respectively, to be compared with the experimental values of 90% and 10% for CO-forming and H-displacement channels, respectively, when assuming an extent of ISC of 90% (Liang et al. 2023b). From our data analysis we reached the conclusion that nearly all HCCN

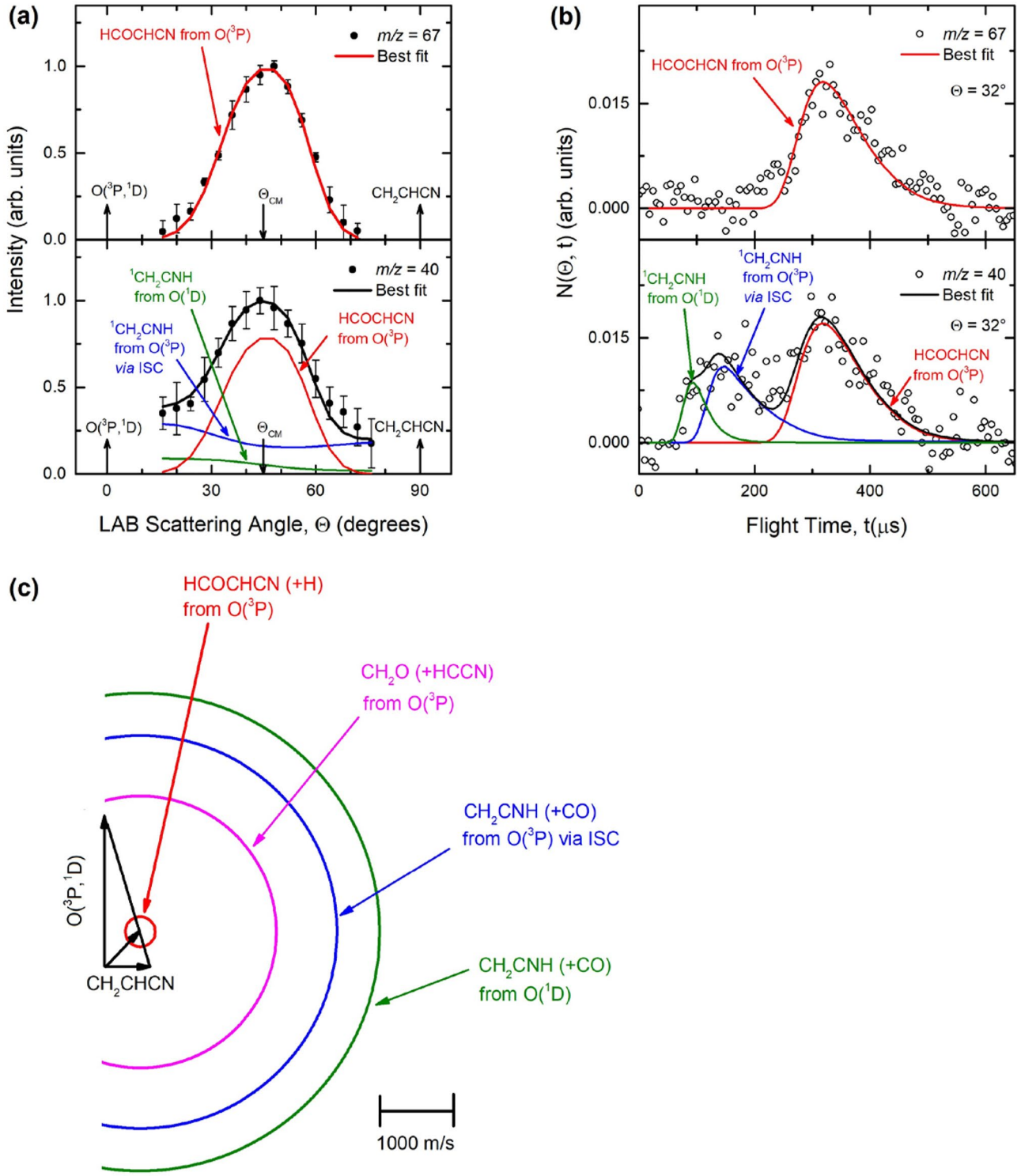

formed from the O(^{3}P) reaction is actually the spin-forbidden excited cyanomethylene, ^{1}HCCN, from channel (2a) reached via ISC from the triplet to the singlet PES, rather than ground-state ^{3}HCCN from the adiabatic channel (1a). That is, the main reaction channel is the C–C bond breaking channel forming CO and ^{1}HCCN, and this means that the three-carbon chain of cyanoacetylene is not maintained when attacked by O(^{3}P) (by an extent of 90%), and this is due to efficient triplet to singlet ISC ($ISC_{t\text{-}s}$) in the entrance channel (see Fig. 1).

However, as discussed in ref. (Liang et al. 2023b) we cannot tell experimentally, within the resolution of our

◂**Fig. 5** **a** LAB angular distribution of (*top*) the HCOCHCN product [channel (10a/10b)] detected at $m/z=67$ (C_3HNO^+), and (*bottom*) the HCOCHCN and CH_2CNH products detected at $m/z=40$ ($C_2H_2N^+$) for the $O(^3P,^1D)+CH_2CHCN$ reactions at $E_c=31.4$ kJ/mol. The filled circles are experimental data (with $\pm1\sigma$ error bars), while the heavy solid black curve represents the calculated total distribution using the best-fit CM functions shown in Fig. 6. Red, blue, and green solid curves (*bottom* panel) represent the separate contributions of the HCOCHCN and CH_2CNH products from channel (10a), (6a), and (6b), respectively, to the calculated total LAB angular distribution. The red curve of HCOCHCN from $O(^3P)$ in the *top* panel corresponds to the red curve in the *bottom* panel. **b** TOF distributions at $\Theta=32°$ of: (*top*) HCOCHCN detected at $m/z=67$, and (*bottom*) HCOCHCN and CH_2CNH detected at $m/z=40$. Empty circles are experimental data, while the red curve for $m/z=67$ and the black curve for $m/z=40$ represent the calculated total distribution using the best-fit functions of Fig. 6. (*bottom*): Red, blue, and green solid curves represent the separate contributions of the labeled products to the total TOF distribution. The red curve of HCOCHCN from $O(^3P)$ in *top* panel corresponds to red curve in the *bottom* panel. **c** Newton diagram of the experiment. The radius of each circle represents the maximum velocity that the indicated products HCOCHCN, CH_2CNH, and CH_2O can attain in the CM system if all available energy is channeled into product recoil energy (see text) (adapted from Pannacci et al. 2023) (color figure online)

experiment, whether additional singlet to triplet ISC is occurring in the exit channel ($ISC_{s\text{-}t}$) (see circle in Fig. 1) that could lead to production of ground state cyanomethylene ^{3}HCCN + CO. Answer to the above question could come from a detailed treatment of ISC in both the entrance and exit channel of the $O(^3P)+HC_3N$ reaction, but this was outside the scope of our work. Interestingly, however, the excited ^{1}HCCN product is expected, in any case, to decay spontaneously to ground state ^{3}HCCN in astrophysical environments [because of an expectedly short phosphorescence lifetime (Szczepaniak 2017)] and, ultimately, the main product of the $O(^3P)+HC_3N$ reaction would be ground state ^{3}HCCN (+CO). This is particularly relevant in astrophysical environments, where it is ground-state ^{3}HCCN that has been actually observed. However, also in combustion environments at atmospheric pressure ^{1}HCCN is expected to be rapidly quenched to ground state ^{3}HCCN.

As shown in Table 1 also for the $O(^1D)$ reaction the dominant product channel is ^{1}HCCN + CO. The BF of 0.94 ± 0.03 was found to agree with the adiabatic calculated value of 0.97. That is, the $O(^1D)$ reaction proceeds adiabatically on the singlet PES. Using the same arguments already invoked in the discussion of the $O(^3P)$ reaction, the ultimate coproduct of CO will be ^{3}HCCN also for the $O(^1D)$ reaction.

Our theoretical results indicated that the main reaction mechanism is addition of $O(^3P)$ to the C1 carbon of the triple C≡C bond of HCC-CN, occurring with an entrance barrier of 9 kJ/mol (see Fig. 1), which makes this reaction relevant not only in combustion environments, but also in relatively warm regions of the ISM, such as circumstellar envelopes and PDRs (photon dominated regions), and, possibly, also the upper atmosphere of Titan, where it could represent an efficient mechanism of formation of cyanomethylene. We emphasize that the main product of the $O(^3P)+HC_3N$ reaction, cyanomethylene (^{3}HCCN), has been detected toward IRC + 10216 where HC_3N is particularly abundant and O atoms are present (Tenenbaum et al. 2006; Agúndez and Cernicharo 2006; Zhang et al. 2017) as well as in the upper atmosphere of Titan (Martens et al. 2008).

Our study led us to propose to include the $O(^3P)$ + cyanoacetylene reaction both as a possible destruction pathway of HC_3N and a possible formation route of HCCN, and also of OCCCN, both in extraterrestrial environments and in the upper atmosphere of Titan. In particular, since both HC_3N and HCCN are present in IRC + 10216, we proposed to search in this environment also for OCCCN (cyanoketyl), which is the other main product of the reaction (see Table 1). We remark that the $O(^3P)+HC_3N$ reaction is not present in astrochemical databases, such as KIDA (Wakelam et al. 2012) and UMIST (McElroy et al. 2013). Finally, we remind that nitriles are key intermediates in the formation of species with biological potential, such as nucleobases and aminoacids, both on Earth and in extraterrestrial environments.

2.3 $O(^3P,^1D)+CH_2CHCN$ (acrylonitrile)

Despite the significant relevance in both astrophysical and combustion environments, very few experimental/theoretical studies existed prior to our recent work (Pannacci et al. 2023) on the $O(^3P,^1D)$ reactions with C_2H_3CN, similarly to the case of the reactions with HC_3N.

According to electronic structure calculations of the relevant triplet and singlet PESs for the $O(^3P)+C_2H_3CN$ reactions from our recent work (Pannacci et al. 2023), there are about ten possible exothermic channels, while several others are nearly thermoneutral or substantially endothermic. The most exothermic ones, which include the two channels (in bold) found to be dominant in our study, are the following:

$O(^3P) + CH_2CHCN$

$\rightarrow {}^1CH_3CN + CO \quad \Delta H^\circ_0 = -463(-478)$ kJ/mol (5a)

$\rightarrow \mathbf{{}^1CH_2CNH + CO} \quad \mathbf{\Delta H^\circ_0 = -348\,(-365)\ kJ/mol}$ **(6a)**

$\rightarrow {}^1OCCHCN + H_2 \quad \Delta H^\circ_0 = -319$kJ/mol (7a)

$\rightarrow {}^2CH_2CN + HCO \quad \Delta H^\circ_0 = -126(-138)$ kJ/mol (8a)

$\rightarrow {}^2COCN + {}^2CH_3 \quad \Delta H^\circ_0 = -69$kJ/mol (9a)

$\rightarrow \mathbf{{}^2HCOCHCN + H} \quad \mathbf{\Delta H^\circ_0 = -62\,(-74)\ kJ/mol}$ **(10a)**

$\rightarrow {}^1CH_2O + {}^3HCCN \quad \Delta H^\circ_0 = -58(-68)$ kJ/mol (11a)

The reported enthalpies of reaction are from electronic structure calculations from Ref. Pannacci et al. (2023) at the CCSD(T)/aug-cc-pVTZ level and at the CCSD(T)/CBS level (values in parentheses) (only for the most relevant channels).

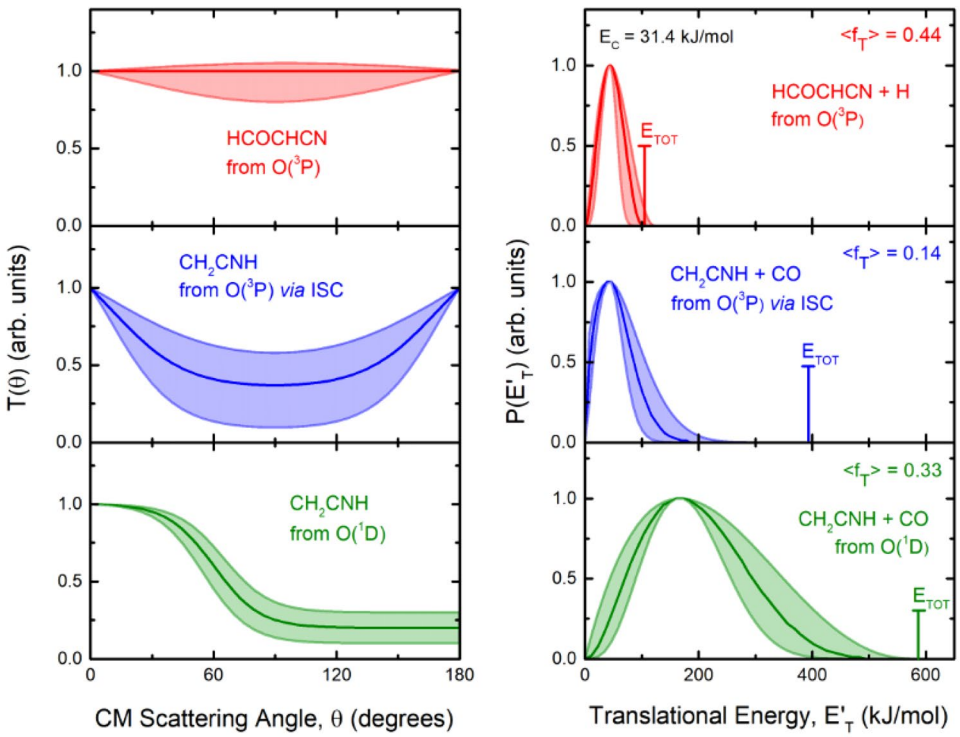

Fig. 6 Best-fit product angular, T(θ), (*left*) and translational energy, P(E′$_T$), (*right*) distributions in the CM reference system for the O(^{3}P,^{1}D) + acrylonitrile reactions. The shaded areas represent the error bars determined for the best-fit CM functions. The vertical arrow in the graphs of P(E′$_T$) indicates the total energy ($E_{TOT} = \Delta H^0_0 - E_c$) for the corresponding reactive channel. The average fraction of the total available energy, for each channel, released as product translational energy, $\langle f_T \rangle$, is also indicated (from Pannacci et al. 2023)

Table 2 Product branching fractions (BFs) for the distinct O(^{3}P) + acrylonitrile and O(^{1}D) + acrylonitrile reactions (at E_c = 31.4 kJ/mol) (from Pannacci et al. 2023)

Reactants	Products	PES involved	Experimental BF
O(^{3}P) + CH_2CHCN	CH_2CNH + CO	Singlet via ISC	0.87 ± 0.05
	HCOCHCN + H	Triplet	0.13 ± 0.05
O(^{1}D) + CH_2CHCN	CH_2CNH + CO	Singlet	dominant (~ 1.0)
	HCOCHCN + H	Singlet	Negligible

The experimental uncertainties of about 40% are indicated

Regarding the O(^{3}P) + acrylonitrile reaction, channel (11a) correlates adiabatically with the triplet PES, while channels (5a)–(9a) are expected to occur on the singlet PES after ISC. Channel (10a) can occur both adiabatically on the triplet PES and via ISC on the singlet PES.

Figure 4 depicts a simplified scheme of the triplet (red lines) and singlet (blue lines) PESs for the reactions O(^{3}P,^{1}D) + CH_2CHCN, where are portrayed only the two most exothermic channels leading to CO formation (5a, 6a), the most exothermic H-displacement channel (10a), and the second most exoergic channel on the triplet PES, that leads to formaldehyde formation (11a). The two bolded product channels are those found to be dominant (Pannacci et al. 2023). In the figure, ISC between the entrance triplet and the underlying singlet PES is indicated with a dotted ellipse. For a more detailed representation of the PESs showing also the other energetically open channels (that, however, were not observed to occur), see Figs. 5 and 6 in Ref. Pannacci et al. (2023).

The corresponding channels (5b)–(10b) for the O(^{1}D) reaction, being 190 kJ/mol more exoergic than the corresponding channels from O(^{3}P), are all strongly exothermic:

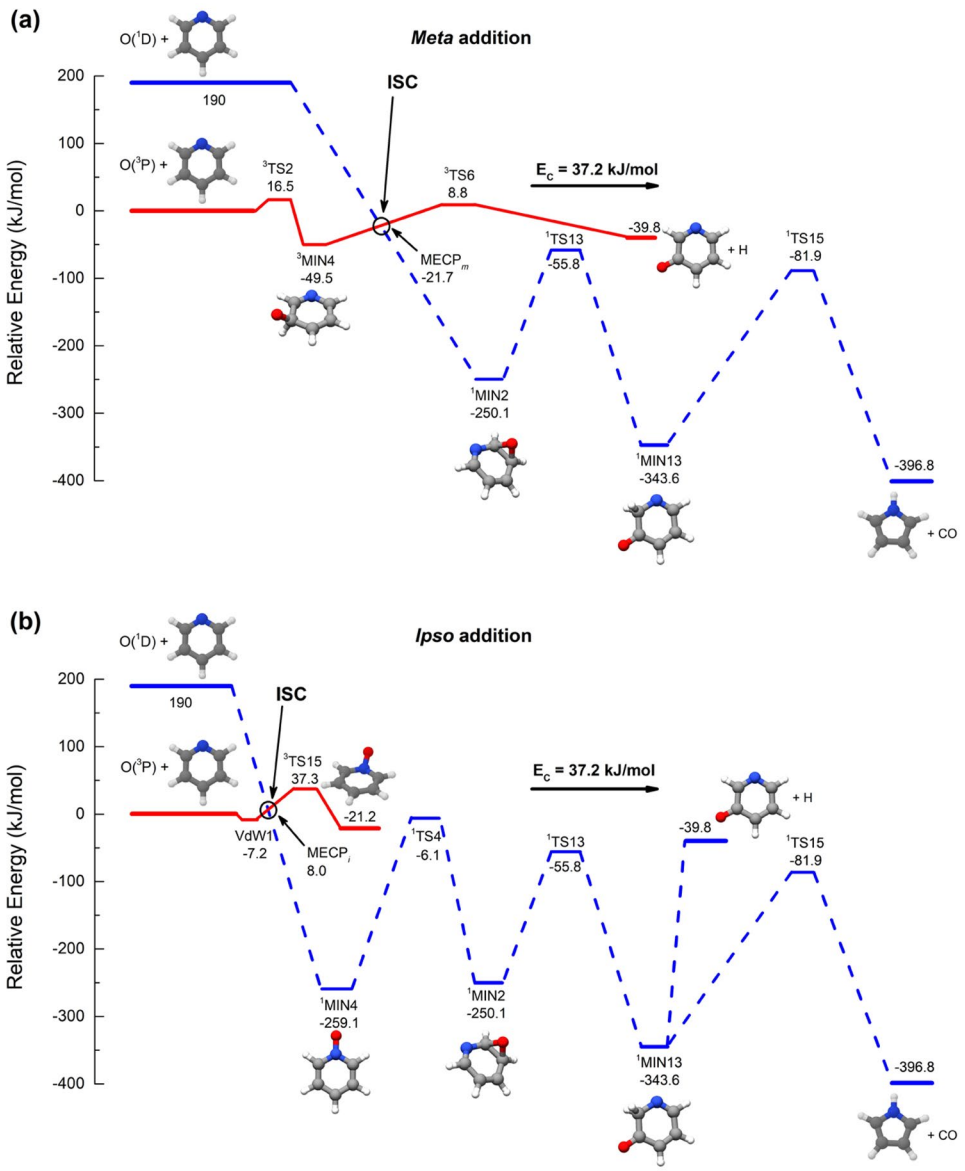

Fig. 7 Simplified representation (schematic) of the triplet (red lines) and singlet (blue lines) PESs of the $O(^3P,^1D)$ + pyridine reaction for $O(^3P)$ *meta* and *ipso* addition. **a** Addition of $O(^3P)$ on the C atom in *meta* position (the most favorable addition site to the ring carbons). **b** *Ipso* addition of $O(^3P)$ on the lone pair of the N atom of pyridine. The location of the minimum energy crossing point (MECP) between triplet and singlet PES following *meta* ($MECP_m$) and *ipso* ($MECP_i$) addition, where ISC occurs, is indicated with a circle. Only the two main observed channels for the $O(^3P)$ reaction are portrayed. The dashed interconversion blue lines on the singlet PES leading to the H and CO forming channels are simplified and qualitative (for a detailed complete view of the triplet/singlet PESs with all the interconversion pathways (maxima and minima) along the full singlet PES, see Recio et al. 2022) (adapted from Recio et al. 2022) (color figure online)

$$
\begin{aligned}
&O(^1D) + CH_2CHCN \\
&\rightarrow {}^1CH_3CN + CO \quad \Delta H_0^\circ = -653(-668)\ \text{kJ/mol} \quad (5b)\\
&\rightarrow \mathbf{^1CH_2CNH + CO} \quad \mathbf{\Delta H_0^\circ = -538\,(-555)\ kJ/mol} \quad \mathbf{(6b)}\\
&\rightarrow {}^1OCCHCN + H_2 \quad \Delta H_0^\circ = -509\ \text{kJ/mol} \quad (7b)\\
&\rightarrow {}^2CH_2CN + HCO \quad \Delta H_0^\circ = -316(-328)\ \text{kJ/mol} \quad (8b)\\
&\rightarrow {}^2COCN + {}^2CH_3 \quad \Delta H_0^\circ = -259\ \text{kJ/mol} \quad (9b)\\
&\rightarrow {}^2HCOCHCN + H \quad \Delta H_0^\circ = -252(-264)\ \text{kJ/mol} \quad (10b)
\end{aligned}
$$

As can be seen from Fig. 4 the two CO forming channels can only be formed on the singlet PES, so they are adiabatic for the $O(^1D)$ reaction, while for the $O(^3P)$ reaction they can only be formed via ISC (see Fig. 4 for the CO channel). In contrast, the HCO, CH_3, and H forming channels can originate from both the triplet and singlet PES. We probed all the above channels, but reactive signal was observed and attributable only to channels (6a)/(6b) and channels (10a)/(10b), that is, the channels leading to CH_2CNH (ketenimine) + CO and to HCOCHCN + H.

Experimentally, reactive scattering signals were detected at $m/z = 68$ ($C_3H_2NO^+$), 67 (C_3HNO^+), 66 (C_3NO^+), 41 ($C_2H_3N^+$), 40 ($C_2H_2N^+$), 39 (C_2HN^+), and 29 (HCO^+). For reasons of S/N ratio, product LAB angular distributions, $N(\Theta)$, and TOF distributions, $N(\Theta, t)$, were measured in detail only for $m/z = 67$ and $m/z = 40$ (using an electron energy of 28 eV), and they are shown in Fig. 5a, b, respectively. Figure 5c depicts, instead, the velocity vector diagram of the experiment, where only the limiting circles of the observed products are indicated. The circle associated to the

CH_2O (+ ^{3}HCCN) product from the O(^{3}P) reaction [channel (11a)] was also added to the Newton diagram because useful in the discussion of the results.

As discussed below, from the experimental data we have characterized channels (6a)/(6b) and (10a)/(10b) by measuring angular and TOF distributions at *m/z* = 67 and 40, respectively, and we have determined their relative yields (BFs). In fact, signal at *m/z* = 68, 67, and 66 was attributed to the H-displacement channel, dominantly from the O(^{3}P) reaction. This because the theoretical predictions of the BFs on the singlet PES clearly indicate a very small contribution of the HCOCHCN + H reactive channel (10b) (BF = 1.2% at the collision energy of the experiment) (see Pannacci et al. 2023). Therefore, we have neglected, within our experimental sensitivity (i.e., BF ≤ 2–3%), the reactive channel (10b). The contribution of HCOCHCN from O(^{3}P) via ISC is very hard to evaluate, but it is expected to be small and, therefore, it was not considered in the data analysis. The measurements on the H-displacement channel were performed at the (− 1) daughter ion (i.e., *m/z* = 67) for reasons of S/N ratio. On the other hand, possible contribution at this *m/z* value from channels (7a)/(7b) (corresponding to H_2 elimination) was ruled out on the basis of the shape of the angular and TOF distributions at this *m/z* ratio (see Pannacci et al. 2023).

As can be seen in Fig. 5a (bottom panel), in contrast to the *m/z* = 67 angular distribution (top panel), the angular distribution at *m/z* = 40 is characterized by a prominent peak centered at around $\Theta_{CM} = 45°$, superimposed on two additional wings. The central peak corresponds to a daughter ion of the HCOCHCN product coming from the H-displacement channel (10a), whose presence is also evident from the slow broad peak in the corresponding *m/z* = 40 TOF spectrum (see Fig. 5b, bottom panel), which is identical to that observed at *m/z* = 67 (Fig. 5b, top panel). The two additional wings in the angular distribution and the fast peaks in the TOF spectra at *m/z* = 40 can be fitted by invoking two other reactive contributions associated with the CO-forming channels (6a) and (6b), observed via the daughter ion $C_2NH_2^+$ of ketenimine (CH_2CNH). The assignment of the signal registered at *m/z* = 40 to ketenimine was made on the basis of the topology of the singlet PES and considering the RRKM/ME predictions of product BFs on the singlet PES (see Pannacci et al. 2023). The situation is similar to what observed in the case of the O(^{3}P,^{1}D) reaction with HC_3N (see Sect. 3.1). In fact, by analyzing the TOF spectra (Fig. 5b), it should be noted that the fingerprint of the $CH_2CNH + CO$ channel from the reaction of O(^{3}P) and O(^{1}D) is particularly clear at the reported angle Θ = 32°. The fact that the angular distribution of CH_2CNH [channels (6a) and (6b)] is much wider than that of HCOCHCN (channel (10a) and that the TOF features associated to the two contributions of CH_2CNH is much faster than that of HCOCHCN, is due to two reasons: (i) the main one is that CH_2CHCN is scattered over a much larger Newton circle (see Fig. 5c) than HCOCHCN because of linear momentum conservation, being its coproduct, CO, much heavier than H; (ii) additionally, channels (6a) and (6b) are much more exothermic than channel (10a). The calculated best-fit LAB angular and TOF distributions for the indicated channels in Fig. 5a, b are obtained from the best-fit CM product angular and translational energy distribution shown, together with their error bounds, in Fig. 6.

Adiabatic statistical calculations of product BFs for the decomposition of the main triplet and singlet intermediates were carried out (Pannacci et al. 2023). Combining experimental and theoretical results, it was concluded that the O(^{3}P) reaction leads to two main product channels, among a variety of possible open channels: (i) CH_2CNH (ketenimine) + CO (dominant, BF = 0.87 ± 0.05), formed via efficient ISC from the entrance triplet PES to the underlying singlet PES, (ii) HCOCHCN + H (minor, BF = 0.13 ± 0.05), occurring adiabatically on the triplet PES. The experimentally derived BFs for both O(^{3}P) and O(^{1}D) reactions are reported in Table 2. As can be seen the derived BFs for O(^{3}P) + acrylonitrile show strong preference for formation of $CH_2CNH + CO$.

Notably, both ketenimine and acrylonitrile have been detected toward the same star-forming regions (as in Sagittarius B2(N) hot core) (Gardner and Winnewisser 1975). Ketenimine is often neglected by astrochemical modelers in the most common astrochemical databases, such as KIDA (Wakelam et al. 2012) and UMIST (Woodall et al. 2007), with respect to its more abundant CH_3CN (acetonitrile) isomer, and also the reaction O(^{3}P) + acrylonitrile is overlooked in models.

It should be noted that the most exothermic of all channels, more than channel (6a), namely, channel (5a) forming $CO + CH_3CN$, is statistically highly unfavored with respect to the isomeric channel (6a) leading to CO + ketenimine because of the much higher interconversion barrier (^{1}TS4) located at − 138 kJ/mol (with respect to reactants) when compared to ^{1}TS3 located at − 235 kJ/mol, that is about 100 kJ/mol lower (see Fig. 4). This is another example where the detailed reaction dynamics, which is dictated by the detailed features of the PES, determines what the most probable product channel actually is, against the common, simplistic and often unwarranted sense often used in models of taking as dominant product channel the most exothermic one.

Our study suggests to include the O(^{3}P) + acrylonitrile reaction both as a possible destruction pathway of CH_2CHCN and a possible formation route of CH_2CNH. The O(^{1}D) + CH_2CHCN reaction mainly leads to formation of $CH_2CNH + CO$ adiabatically on the singlet PES (see Table 2). This result can improve models related to the chemistry of interstellar ices

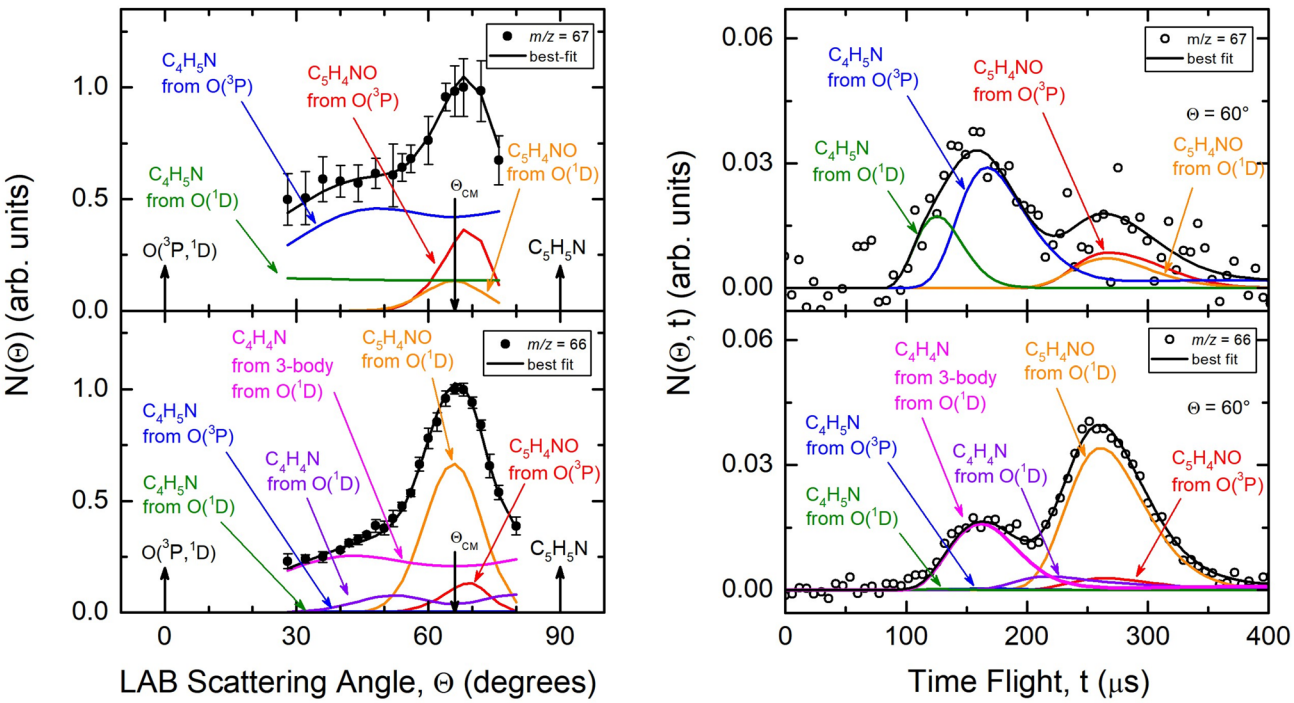

Fig. 8 (*lhs*): Comparison of the LAB angular distributions at $m/z = 67$ [parent ion of pyrrole product and (-27) daughter ion of pyridoxyl product] and at $m/z = 66$ [(-1) daughter ion of pyrrole, parent ion of pyrrolyl, and (-28) daughter ion of pyridoxyl] for the $O(^3P,^1D)$ + pyridine reaction at $E_c = 37.2$ kJ/mol. (*rhs*): TOF distributions at the two same masses, at the LAB angle of 60°. The black solid lines over the experimental points on both angular and TOF distributions are the global calculated best-fit curves when using the weighted best-fit CM product angular and translational energy distributions (see Fig. 4 in the Supporting Information of Ref. Recio et al. 2022). The distinct contributions of the various products from the distinct $O(^3P)$ and $O(^1D)$ reactions are indicated and color coded (adapted from Recio et al. 2022)

and cometary comas, where $O(^1D)$ reactions are believed to play an important role. Overall, our results are expected to be useful to improve models of combustion and extraterrestrial environments.

2.4 $O(^3P,^1D) + C_6H_5N$ (pyridine)

Recent CMB experiments backed by theoretical calculations of the reaction PESs and of product distributions on multichannel $O(^3P)$ reactions with a variety of unsaturated hydrocarbons containing 2C, 3C, and 4C atoms (simple alkynes, alkenes, dienes, and conjugated dienes) and with simple aromatic hydrocarbons (benzene, toluene) have shown that ISC between the weakly coupled entrance triplet and underlying singlet PESs plays a central role in the dynamics and kinetics of these reactions (Casavecchia et al. 2015; Pan et al. 2017; Caracciolo et al. 2019c; Vanuzzo et al. 2021; Cavallotti et al. 2022). These $O(^3P)$ reactions were all found to mainly proceed via an *addition–elimination* mechanism and to exhibit from a small to a sizeable entrance energy barrier (from a few kJ/mol up to 20 kJ/mol). In all these reactions the electrophilic addition of $O(^3P)$ to the unsaturated bond(s) leads to a covalently bound triplet diradical intermediate(s) in the triplet PES. Since triplet and singlet PESs always cross in these systems, a nonadiabatic jump (ISC) can occur from the entrance triplet PES to the underlying singlet PES. It was found that ISC takes place near the minimum

Table 3 Product branching fractions (BFs) for the distinct $O(^3P)$ + pyridine and $O(^1D)$ + pyridine reactions at $E_c = 37.2$ kJ/mol (adapted from Recio et al. 2022)

Reactants	Products	PES involved	Experimental BF
$O(^3P) + C_5H_5N$	$C_5H_4NO + H$	Triplet	$0.02^{+0.02}_{-0.01}$
	$C_4H_5N + CO$	Singlet via ISC	$0.98^{+0.01}_{-0.02}$
$O(^1D) + C_5H_5N$	$C_5H_4NO + H$	Singlet	0.014 ± 0.007
	$C_4H_5N + CO$	Singlet	0.16 ± 0.08
	$C_4H_4N + H + CO$	Singlet	0.78 ± 0.10
	$C_4H_4N + HCO$	Singlet	0.04 ± 0.02

of the initial triplet intermediate (more than one intermediate can be present when three or more C atoms are present in the molecule), which is reached only after the triplet entrance barrier has been surmounted. In these systems, ISC mainly affects the number of exit channels and the BFs of the various product channels. The extent of ISC usually increases with increasing *lifetime* of the triplet intermediate, which, in turn, typically increases with increasing stability of the diradical and lowering of the collision energy (Pan et al. 2017). Interestingly, when we studied the reaction of $O(^3P)$ with one of the simplest heterocyclic molecules, namely pyridine, which is isoelectronic with benzene, and compared the two systems, we observed a hitherto unobserved ISC-based mechanism (Recio et al. 2022). The study of the $O(^3P)$ + pyridine reaction was motivated by the importance of this system in several fields including biology, combustion, and astrochemistry (Wang et al. 2012; Parker et al. 2015; Puzzarini and Barone 2020). Specifically, we found that ISC does occur for *ortho*-, *meta*-, and *para*-addition of the O atom to the carbons of the aromatic ring of pyridine, after the corresponding entrance barrier has been surmounted, as in the case of the reaction of $O(^3P)$ with the isoelectronic molecule of benzene. However, for these types of addition the extent of ISC was found to be small, while it was found that ISC can also occur, much more efficiently, for O atom addition to the heteroatom, specifically, to the lone pair of the nitrogen atom (*ipso* addition) before the entrance barrier. Figure 7 shows a simplified, schematic representation of the triplet/singlet PESs for *meta* and *ipso* addition of $O(^3P)$ to pyridine. In the figure we emphasize the minimum energy crossing point (MECP) for the two cases of *ipso* and *meta* addition ($MECP_i$ and $MECP_m$, respectively), and portray schematically only the pathways to the main product channels of the $O(^3P) + C_5H_5N$ reaction, namely, the strongly exothermic spin-forbidden CO elimination channel, involving ring-contraction with formation of pyrrole + CO, occurring on the singlet PES reached from the triplet PES via ISC, and the H-displacement channel occurring adiabatically on the triplet PES or, nonadiabatically (via ISC), on the singlet PES, and leading to the weakly exothermic pyridoxyl + H products. The fact that ISC is much more efficient for *ipso* addition than for *meta* addition is due to the fact that the MECP for ISC in the case of *ipso* addition is located at an energy (8.0 kJ/mol) lower than the entrance barrier (16.5 kJ/mol) for *meta* addition (the most favourable addition site to the ring C among the three possible *ortho*, *meta*, and *para* sites) (Fig. 7). The CMB experiments were supported by detailed theoretical work, consisting in high-level, quantum electronic structure calculations of the triplet and singlet PESs and related RRKM/ME simulations of product BFs, with the inclusion of ISC for both *meta* (the preferred attack position on the C sites) and *ipso* addition (to the N atom) (Recio et al. 2022). The theoretical calculations of the triplet and singlet PESs for the $O(^3P,^1D)$ + pyridine reaction indicated that the main energetically allowed product channels at $E_c = 37.2$ kJ/mol for the $O(^3P)$ reaction are (in bold are the two main observed channels):

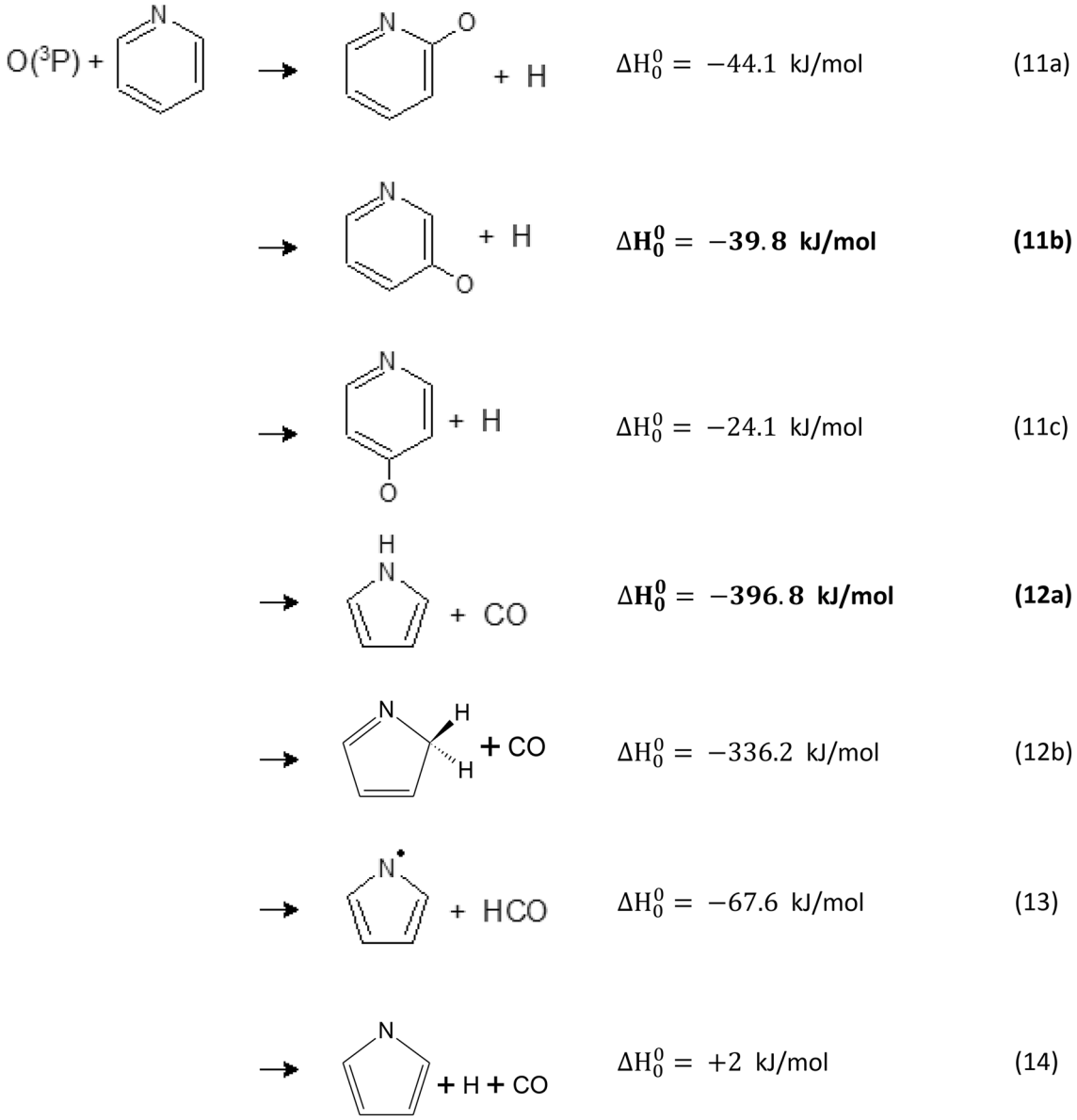

$\Delta H_0^0 = -44.1$ kJ/mol (11a)

$\mathbf{\Delta H_0^0 = -39.8\ kJ/mol}$ **(11b)**

$\Delta H_0^0 = -24.1$ kJ/mol (11c)

$\mathbf{\Delta H_0^0 = -396.8\ kJ/mol}$ **(12a)**

$\Delta H_0^0 = -336.2$ kJ/mol (12b)

$\Delta H_0^0 = -67.6$ kJ/mol (13)

$\Delta H_0^0 = +2$ kJ/mol (14)

These same channels can also be formed from the $O(^1D) + C_5H_5N$ reaction, with the reaction exothermicities in this case being larger by 190 kJ/mol because of the energy difference between excited state ^1D and ground state ^3P of atomic oxygen. It should be noted that while the *o*-, *m*-, and *p*-pyridoxyl + H products can be formed on either triplet or singlet PES, the pyrrole + CO products can be formed from $O(^3P)$ only via ISC from the entrance triplet PES to the singlet PES, or from $O(^1D)$ adiabatically. Particularly relevant to the $O(^1D)$ reaction, besides the H and CO forming channels, are also the so called "3-body channel" (14), generated by the fast uni-molecular decay of internally hot pyrrole before reaching the detector, and the channel (13) leading to pyrrolyl + HCO, that for $O(^1D)$ are both strongly exothermic.

In the following we summarize the main experimental results and findings of our recent study. The $O(^3P,^1D) + C_5H_5N$ reactions were investigated in CMB experiments at $E_c = 37.2$ kJ/mol using a supersonic oxygen beam containing about 90% of $O(^3P)$ and 10% of $O(^1D)$ (Alagia et al. 1997). Data analysis was carried out in a similar way as for the related $O(^3P,^1D) + C_6H_6$ (benzene) reaction (Vanuzzo et al. 2021). Notably, it was found that there are similarities as well as differences in the derived best-fit CM functions for the related $O(^3P,^1D)$ + pyridine and $O(^3P,^1D)$ + benzene systems (Recio et al. 2022).

Reactive scattering signals were observed at $m/z = 94$ ($C_5H_4NO^+$), 93 ($C_5H_3NO^+$), 67 ($C_4H_5N^+$), and 66 ($C_4H_4N^+$). From LAB product angular and TOF distribution measurements at $m/z = 94$, 67, and 66, we characterized the occurrence of the H-displacement channel(s), from data at $m/z = 67$ the pyrrole formation channels as well as the H-displacement channel(s), and from data at $m/z = 66$ the 3-body and HCO channels, as well as the H-displacement channel(s). In Fig. 8 we show some data at $m/z = 66$ and 67 (the angular distributions, N(Θ), and exemplary TOF distributions, N(Θ,t), at the LAB angle of 60°), to demonstrate the dynamics of the observed reaction channels from O(^{3}P) and O(^{1}D) reactions (for the complete data set, see Recio et al. 2022).

As mentioned above, the C_5H_4NO (pyridoxyl) product, besides at the parent ion ($m/z = 94$), was also detected (more readily) at $m/z = 66$ and also at $m/z = 67$, originating from strong dissociative ionization of the parent ion $C_5H_4NO^+$ in the ionizer. As can be seen in Fig. 8(*lhs*) the N(Θ)s of $m/z = 66$ and 67 exhibit a pronounced, slightly backward-biased distribution with respect to the O atom direction, centered around the CM angle. The N(Θ) of the C_5H_4NO products at $m/z = 94$ (not shown here—see supporting Fig. 1 in Recio et al. 2022) and their contributions at $m/z = 66$ and 67 are confined to a narrow LAB angular range because of linear momentum conservation, as the H coproduct is very light. However, in contrast to the $m/z = 94$ N(Θ), at both $m/z = 66$ and 67, while the partial contribution of the coproduct of the H displacement channel has the same shape as at $m/z = 94$, a strong reactive signal is also present at LAB angles well outside the range where the heavy coproducts of H channels are confined, thus suggesting the presence of at least another channel, besides the H channel. The different channels were identified from the combined analysis of angular and TOF distributions; in particular the TOF spectra N(Θ,t), although are essentially bimodal [see Fig. 8 (*rhs*)], carry the fingerprint of all observed channels mentioned above [two from O(^{3}P) and four from O(^{1}D)] (see Recio et al 2022 for the complete data set and analysis).

Quantitative information on the reaction dynamics was obtained by moving from the LAB coordinate system to the CM reference frame and analyzing the best-fit product T(θ) and P(E_T') distributions. In Fig. 8 the solid curves superimposed on the experimental distributions are the calculated curves obtained using the best-fit CM T(θ) and P(E_T') functions reported in supporting Fig. 4 of Recio et al. (2022) for all six observed channels [the two channels from O(^{3}P) and the four from O(^{1}D)].

The procedure adopted to determine reaction yields (product BFs) for this system was similar to that used for the O(^{3}P,^{1}D) + C_6H_6 system (Vanuzzo et al. 2021). Despite the large number of exothermic channels, our study (Recio et al. 2022) showed that the dominant product channels from the O(^{3}P) reaction are only channels (11b) and (12a), leading to H and CO elimination, respectively, with channel (11b) being minor (BF = $0.02^{+0.02}_{-0.01}$) and coming from the triplet PES via adiabatic reaction, and channel (12a) being dominant (BF = $0.98^{+0.01}_{-0.02}$ and coming from the singlet PES via efficient triplet to singlet ISC. The product BFs for both O(^{3}P) and O(^{1}D) reactions are summarized in Table 3. The fact that the BF of the pyrrole + CO channel from O(^{3}P) is 0.98 indicates that the extent of ISC is very large (98%).

The O(^{3}P) + pyridine reaction is the system with the largest contribution of triplet to singlet ISC observed up to now, a feature that theory explained with the occurrence of ISC in the entrance channel for the *ipso* addition of O(^{3}P) to the lone pair of the nitrogen atom, before the entrance barrier (Recio et al. 2022). Instead, for the O(^{1}D) reaction the main product channel is the three-body channel leading to pyrrolyl + H + CO (BF = 0.78 ± 0.10), which, while nearly thermoneutral for O(^{3}P) [channel (14)], is strongly exothermic for O(^{1}D) ($\Delta H_0^0 = -188$ kJ/mol). Notably, the 3-body channel was also observed to be the main channel, leading to cyclopentadiene + H + CO, in the corresponding reaction of O(^{1}D) with benzene (Vanuzzo et al 2021). For O(^{1}D), the pyrrole + CO channel has BF = 0.16 ± 0.08, the H channel has BF = 0.014 ± 0.007, and the HCO-forming channel has BF = 0.04 ± 0.02 (see Table 3). This indicates that, overall, also for the O(^{1}D) reaction the H-displacement channel is minor.

The experimentally estimated extent of ISC of about 98% is in sharp contrast to what was derived for the reaction of O(^{3}P) with the isoelectronic benzene molecule, where the extent of ISC was determined to be *ca.* 50% at a comparable E_c (Vanuzzo et al. 2021). In O(^{3}P) + benzene, the H + C_6H_5O (phenoxy) production is controlled by the spin-allowed triplet pathway with BF = 0.66 (0.48 from the adiabatic contribution on the triplet PES and 0.18 from the nonadiabatic contribution on singlet PES via ISC), that is, it is much larger than in O(^{3}P) + pyridine. The ring contraction channel leading to CO + C_5H_6 (cyclopentadiene) occurs via triplet to singlet ISC with a BF of 0.32, that is, the ring contraction channel in O(^{3}P) + benzene is much smaller (50%) than in O(^{3}P) + pyridine (98%).

The observation that ISC to the singlet PES, leading to formation of pyrrole + CO [both 1H- and 2H-pyrrole (channel (12a) and (12b), respectively) in a 1/2.4 ratio, according to statistical calculations (Recio et al. 2022)], occurs in the entrance channel before the barrier, following the *ipso* interaction between the O atom and the lone

pair of the N atom of pyridine on the triplet PES, represented the first detection of ISC in the entrance channel of a bimolecular reaction in the absence of heavy atoms (e.g., iodine). Interestingly, this reaction mechanism involving ISC before the entrance barrier may play a role in bimolecular reactions with the same characteristics. In particular, considering that important biomolecules, including nucleobases, are N-heterocyclic aromatic compounds, the finding of our study on the reaction of $O(^3P)$ with pyridine about the key role of the electrophilic attack of the oxygen atom on the nitrogen atom accompanied by efficient ISC, as opposed to the usual attack on the carbons of the aromatic ring, may have significant implications in biological processes. Finally, in relation to the potential astrochemical relevance of the $O(^3P)$ + pyridine reaction, our results suggested a possible destruction pathway of pyridine hitherto unobserved in different environments of the interstellar medium.

3 Conclusions and outlook

We have reviewed the recent contributions made by CMB studies in our laboratory of the bimolecular reactions of ground and excited state oxygen atoms, $O(^3P)$ and $O(^1D)$, with the two simplest unsaturated nitriles, cyanoacetylene and cyanoethylene, and the simplest N-heterocyclic molecule, pyridine. The primary products of these multichannel reactions and their product branching fractions have been determined under well-defined energetic conditions. With the assistance of synergistic calculations of the relevant PESs and of statistical (RRKM/ME) calculations, in the conditions of the experiments, of product BFs, the detailed reaction mechanisms have been elucidated and the central role played by intersystem-crossing in the $O(^3P)$ reactions has been assessed. Specifically, ISC has been found to control the product distributions in all these reactions. The contributions of these studies to the modelling, and therefore to a deeper comprehension of combustion and astrochemical processes have been discussed.

We emphasize that the characterization of multichannel bimolecular neutral–neutral reactions of relevance in combustion and astrochemistry is a challenging endeavour that certainly call for a multidisciplinary approach. Because kinetic experiments are seldom able to determine all the primary products and their branching fractions at the temperatures of relevance in these environments, dynamical experiments using the CMB technique with *universal* MS detection, empowered with *soft* electron-ionization (or *soft* VUV photo-ionization), have revealed to be a powerful and most valuable tool, complementary to kinetic experiments, to provide product BFs in specific energy (temperature) conditions. The CMB experiments, combined with high-level theoretical calculations of the relevant reaction PESs and statistical (RRKM/ME) computations of product BFs with inclusion of nonadiabatic effects (ISC) can ultimately lead to the predictions of both the global reaction rate constant and the channel-specific rate constants as a function of temperature (and also pressure), that are the needed quantities for improving combustion and astrochemical models. We emphasize that the detailed comparison between theoretical predictions of product BFs of a multichannel reaction, using coupled potential energy surfaces with inclusion of ISC effects, with the experimental product BFs provides a sensitive test of the reliability of the underlying reaction PESs. When the PESs are validated by a good accord between experiment and theory, then theory can be used to predict product BFs as well as channel-specific rate constants as a function of temperature, which may range from the low values of cold molecular clouds to those of the atmosphere of Titan, up to those of combustion processes. Up to now this approach has been very rewarding when applied to a large variety of reactions of oxygen atoms with unsaturated aliphatic and aromatic hydrocarbons as well as the present N-bearing molecules.

We are currently extending in our laboratory similar combined CMB and theoretical investigations to also reaction involving, besides oxygen atoms also sulfur atoms, alkyl radicals and other molecular species of relevance in combustion and astrochemistry, such as alkyl-benzenes, other heterocyclic molecules, and the prototype of polycyclic aromatic hydrocarbons, such as naphthalene. Combustion and astrochemical models are expected to benefit from the additional, detailed information that can be obtained from studies such as those described here. New insights and better understanding of these complex environments can ultimately be expected.

Acknowledgements Work supported by MUR (PRIN 2017, MAGIC DUST, Prot. 2017PJ5XXX; Department of Excellence-2018-2022-Project AMIS) and Italian Space Agency (ASI, DC-VUM-2017-034, Grant no. 2019-3 U.O Life in Space). We thank all the coworkers who have contributed to the different parts of the research summarized in this short review.

Funding Open access funding provided by Università degli Studi di Perugia within the CRUI-CARE Agreement.

Declarations

Conflict of interest Authors declare no competing financial interests.

References

Agúndez M, Cernicharo J (2006) Oxygen chemistry in the circumstellar envelope of the carbon-rich star IRC+10216. Astrophys J 650:374–393

Aladro R, Martín-Pintado J, Martín S, Mauersberger R, Bayet E (2011) CS, HC_3N, and CH_3CCH multi-line analysest toward starburst galaxies. Astron Astrophys 525:A89

Aladro R, Martín S, Riquelme D, Henkel C, Mauersberger R, Martín-Pintado J, Weiß A, Lefevre C, Kramer C, Requena-Torres MA et al (2015) Lambda = 3 mm line survey of nearby active galaxies. Astron Astrophys 579:A101

Alagia M, Balucani N, Casavecchia P, Stranges D, Volpi GG (1993a) Crossed beam studies of four-atom reactions: the dynamics of OH + D_2. J Chem Phys 98:2459–2462

Alagia M, Balucani N, Casavecchia P, Stranges D, Volpi GG (1993b) Crossed beam studies of four-atom reactions: the dynamics of OH + CO. J Chem Phys 98:8341–8344

Alagia M, Balucani N, Casavecchia P, Stranges D, Volpi GG (1995) Reactive scattering of atoms and radicals. J Chem Soc Faraday Trans 91:575–596

Alagia M, Balucani N, Cartechini L, Casavecchia P, van Kleef EH, Volpi GG, Aoiz FJ, Bañares L, Schwenke DW, Allison TC, Mielke SL, Trulhar DG (1996) Dynamics of the simplest chlorine atom reaction: an experimental and theoretical study. Science 273:1519–1522

Alagia M, Aquilanti V, Ascenzi D, Balucani N, Cappelletti D, Cartechini L, Casavecchia P, Pirani F, Sanchini G, Volpi GG (1997) Magnetic analysis of supersonic beams of atomic oxygen, nitrogen, and chlorine generated from a radio-frequency discharge. Isr J Chem 37:329–342

Albert DR, Davis HF (2013) Studies of bimolecular reaction dynamics using pulsed high-intensity vacuum-ultraviolet lasers for photoionization detection. Phys Chem Chem Phys 15:14566–14580

Balucani N, Beneventi L, Casavecchia P, Stranges D, Volpi GG (1991) Effect of reagent electronic excitation on the dynamics of chemical reactions: a high resolution crossed beam study of O(^{3}P,^{1}D) + H_2S. J Chem Phys 94:8611–8614

Balucani N, Alagia M, Cartechini L, Casavecchia P, Volpi GG, Sato K, Takayanagi T, Kurosaki Y (2000) Cyanomethylene formation from the reaction of excited nitrogen atoms with acetylene: a crossed beam and ab initio study. J Am Chem Soc 122:4443–4450

Balucani N, Capozza G, Leonori F, Segoloni E, Casavecchia P (2006) Crossed molecular beam reactive scattering: from simple triatomic to multichannel polyatomic reactions. Int Rev Phys Chem 25:109–163

Balucani N, Bergeat A, Cartechini L, Volpi GG, Casavecchia P, Skouteris D, Rosi M (2009) Combined crossed molecular beam and theoretical studies of the N(^{2}D) + CH_4 reaction and implications for atmospheric models of Titan. J Phys Chem A 113:11138–11152

Balucani N, Leonori F, Petrucci R, Stazi M, Skouteris D, Rosi M, Casavecchia P (2010) Formation of nitriles and imines in the atmosphere of Titan: combined crossed-beam and theoretical studies on the reaction dynamics of excited nitrogen atoms N(^{2}D) with ethane. Faraday Discuss 147:189–216

Balucani N, Skouteris D, Leonori F, Petrucci R, Hamberg M, Geppert WD, Casavecchia P, Rosi M (2012) Combined crossed beam and theoretical studies of the N(^{2}D) + C_2H_4 reaction and implications for atmospheric models of Titan. J Phys Chem A 116:10467–10479

Balucani N, Leonori F, Casavecchia P, Fu B, Bowman JM (2015a) Crossed molecular beams and quasiclassical trajectory surface hopping studies of the multichannel nonadiabatic O(^{3}P) + ethylene reaction at high collision energy. J Phys Chem A 119:12498–12511

Balucani N, Leonori L, Petrucci R, Wang X, Casavecchia P, Skouteris D, Albernaz AF, Gargano R (2015b) A combined crossed molecular beam and theoretical study of the reaction CN + C_2H_4. Chem Phys 449:34–42

Balucani N, Caracciolo A, Vanuzzo G, Skouteris D, Rosi M, Pacifici L, Casavecchia P, Hickson KM, Loison JC, Dobrijevic M (2023) An experimental and theoretical investigation of the N(^{2}D) + C_6H_6 (benzene) reaction with implications for the photochemical models of Titan. Faraday Discuss 245:327–351

Balucani N, Vanuzzo G, Recio P, Caracciolo A, Rosi M, Cavallotti C, Casavecchia P (2024) Crossed molecular beam experiments on the multichannel reaction of toluene with atomic oxygen and theoretical simulations. Faraday Discuss **(to be submitted)**

Beneventi L, Casavecchia P, Volpi GG (1986a) Observation of high frequency quantum oscillations in elastic differential cross sections: a critical test of the Ne–Ar interaction potential. J Chem Phys 84:4828–4832

Beneventi L, Casavecchia P, Volpi GG (1986b) High-resolution total differential cross sections for scattering of helium by O_2, N_2 and NO. J Chem Phys 85:7011–7029

Berteloite C, Le Picard SD, Sims IR, Rosi M, Leonori F, Petrucci R, Balucani N, Wang X, Casavecchia P (2011) Low temperature kinetics, crossed beam dynamics and theoretical studies of the reaction S(^{1}D) + CH_4 and low temperature kinetics of S(^{1}D) + C_2H_2. Phys Chem Chem Phys 13:8485–8501

Biver N, Bockelee-Morvan D, Moreno R, Crovisier J, Colom P, Lis DC, Sandqvist A, Boissier J, Despois D, Milam SN (2015) Ethyl alcohol and sugar in comet C/2014 Q2 (Lovejoy). Sci Adv 1:e1500863

Boato G, Volpi GG (1999) Experiments on the dynamics of molecular processes: a chronicle of fifty years. Annu Rev Phys Chem 50:23–50

Bockelée-Morvan D, Lis DC, Wink JE, Despois D, Crovisier J, Bachiller R, Benford DJ, Biver N, Colom P, Davies JK et al (2000) New molecules found in comet C/1995 O1 (Hale-Bopp)—investigating the link between cometary and interstellar material. Astron Astrophys 353:1101–1114

Brandenburg CF, Latham DR (1968) Spectroscopic identification of basic nitrogen compounds in Wilmington petroleum. J Chem Eng Data 13:391–394

Capozza G, Segoloni E, Leonori F, Volpi GG, Casavecchia P (2004) Soft electron impact ionization in crossed molecular beam reactive scattering: the dynamics of the O(^{3}P) + C_2H_2 reaction. J Chem Phys 120:4557–4560

Caracciolo A, Vanuzzo G, Balucani N, Stranges D, Pratali Maffei L, Cavallotti C, Casavecchia P (2019a) Combined experimental and

theoretical studies of the $O(^3P)$ + 1-butene reaction dynamics: Primary products, branching ratios and role of intersystem crossing. J Phys Chem A 123:9934–9956

Caracciolo A, Vanuzzo G, Balucani N, Stranges D, Tanteri S, Cavallotti C, Casavecchia P (2019b) Crossed molecular beams and theoretical studies of the $O(^3P)$ + 1,2-butadiene reaction: dominant formation of propene + CO and ethylidene + ketene molecular channels. Chin J Chem Phys 32:113–122

Caracciolo A, Vanuzzo G, Recio P, Balucani N, Casavecchia P (2019c) Molecular beam studies of elementary reactions relevant in plasma/combustion chemistry: $O(^3P)$ + unsaturated hydrocarbons. Rend Fis Acc Lincei 30:549–561

Casavecchia P (2000) Chemical reaction dynamics with molecular beams. Rep Prog Phys 63:355–414

Casavecchia P, Balucani N, Alagia M, Cartechini L, Volpi GG (1999a) Reactive scattering of oxygen and nitrogen atoms. Acc Chem Res 32:503–511

Casavecchia P, Balucani N, Volpi GG (1999b) Crossed beam studies of reaction dynamics. Annu Rev Phys Chem 50:347–376

Casavecchia P, Balucani N, Cartechini L, Capozza G, Bergeat A, Volpi GG (2001) Crossed beam studies of elementary reactions of N and C atoms and CN radicals of importance in combustion. Faraday Discuss 119:27–49

Casavecchia P, Capozza G, Segoloni E, Leonori F, Balucani N, Volpi GG (2005) Dynamics of the $O(^3P)$ + C_2H_4 reaction: identification of five primary product channels (vinoxy, acetyl, methyl, methylene, and ketene) and branching ratios by the crossed molecular beam technique with soft electron ionization. J Phys Chem A 109:3527–3530

Casavecchia P, Leonori F, Balucani N, Petrucci R, Capozza G, Segoloni E (2009) Probing the dynamics of polyatomic multichannel elementary reactions by crossed molecular beam experiments with soft electron-ionization mass spectrometric detection. Phys Chem Chem Phys 11:46–65

Casavecchia P, Liu K, Yang X (2010) Reactive scattering: reactions in three dimensions. In: Brouard M, Vallance C (eds) Tutorials in molecular reaction dynamics, vol 6. Royal Society of Chemistry Publishing, Cambridge, pp 167–213

Casavecchia P, Leonori F, Balucani N (2015) Reaction dynamics of oxygen atoms with unsaturated hydrocarbons from crossed molecular beam studies: primary products, branching ratios and role of intersystem crossing. Int Rev Phys Chem 34:161–204

Cavallotti C, Leonori F, Balucani N, Nevrly V, Bergeat A, Falcinelli S, Vanuzzo G, Casavecchia P (2014) Relevance of the channel leading to formaldehyde + triplet ethylidene in the $O(^3P)$ + propene reaction under combustion conditions. J Phys Chem Lett 5:4213–4218

Cavallotti C, De Falco C, Pratali Maffei L, Caracciolo A, Vanuzzo G, Balucani N, Casavecchia P (2020) A theoretical study of the extent of intersystem crossing in the $O(^3P)$ + C_6H_6 reaction with experimental validation. J Phys Chem Lett 11:9621–9628

Cavallotti C, Della Libera A, Recio P, Caracciolo A, Balucani N, Casavecchia P (2022) Crossed-beam and theoretical studies of multichannel nonadiabatic reactions: branching fractions and role of intersystem crossing for $O(^3P)$ + 1,3-butadiene. Faraday Discuss 238:161–182

Ceccarelli C, Caselli P, Fontani F, Neri R, López-Sepulcre A, Codella C, Feng S, Jiménez-Serra I, Lefloch B, Pineda JE et al (2017) Seeds of life in space (SOLIS): the organic composition diversity at 300–1000 au scale in solar-type star-forming regions. Astrophys J 850:176

Chapillon E, Dutrey A, Guilloteau S, Piétu V, Wakelam V, Hersant F, Gueth F, Henning T, Launhardt R, Schreyer K et al (2012) Chemistry in disks. VII. First detection of HC_3N in protoplanetary disks. Astrophys J 756:58

Chen W, Wang R, Yuan D, Zhao H, Luo C, Tan Y, Li S, Zhang DH, Wang X, Sun Z, Yang X (2021) Quantum interference between spin-orbit split partial waves in the F + HD→HF + D reaction. Science 371:936–940

Costagliola F, Aalto S, Rodriguez MI, Muller S, Spoon HWW, Martín S, Peréz-Torres MA, Alberdi A, Lindberg JE, Batejat F et al (2011) Molecules as tracers of galaxy evolution: an EMIR survey. Astron Astrophys 528:A30

Cvetanović RJ (1955) Reaction of oxygen atoms with ethylene. J Chem Phys 23:1375–1380

Daly NR (1960) Scintillation type mass spectrometer ion detector. Rev Sci Instrum 31:264–267

de Aragão EVF, Faginas-Lago N, Rosi M, Mancini L, Balucani N, Skouteris D (2020) A computational study of the reaction cyanoacetylene and cyano radical leading to 2-butynedinitrile and hydrogen radical. Lect Notes Artif Intell 12251:707–716

de Aragão EVF, Mancini L, Faginas-Lago N, Rosi M, Balucani N, Pirani F (2021) Long-range complex in the HC_3N + CN potential energy surface: ab initio calculations and intermolecular potential. Lect Notes Artif Intell 12958:413–425

de Aragão EVF, Mancini L, Faginas-Lago N, Rosi M, Skouteris D, Pirani F (2022) Semiempirical potential in kinetics calculations on the HC_3N + CN reaction. Molecules 27:2297

de Aragão EVF, Liang P, Mancini L, Marchione D, Vanuzzo G, Faginas-Lago N, Rosi M, Skouteris D, Ferlin F, Pirani F, Casavecchia P, Balucani N (2024) Combined crossed molecular beam and theoretical studies on the cyanoacetylene (HC_3N) + CN($X^2\Sigma^+$) reaction. Astron Astrophys **(in preparation)**

Endo Y, Tsuchiya S, Yamada C, Hirota E, Koda S (1986) Microwave kinetic spectroscopy of reaction intermediates: O + ethylene reaction at low pressure. J Chem Phys 85:4446–4452

Finlayson-Pitts BJ, Pitts JN Jr (1986) Atmospheric chemistry—fundamentals and experimental techniques. Wiley, New York

Fu B, Han YC, Bowman JM, Angelucci L, Balucani N, Leonori F, Casavecchia P (2012a) Intersystem crossing and dynamics in $O(^3P)$ + C_2H_4 multichannel reaction: experiment validates theory. Proc Natl Acad Sci 109:9733–9738

Fu B, Han YC, Bowman JM, Leonori F, Balucani N, Angelucci L, Occhiogrosso A, Petrucci R, Casavecchia P (2012b) Experimental and theoretical studies of the $O(^3P)$ + C_2H_4 reaction dynamics: collision energy dependence of branching ratios and extent of intersystem crossing. J Chem Phys 137:22A532

Gardner FF, Winnewisser G (1975) The detection of interstellar vinylcyanide/acrylonitrile. Astrophys J 195:L127–L130

Geppert WD, Naulin C, Costes M, Capozza G, Cartechini L, Casavecchia P, Volpi GG (2003) Combined crossed-beam studies of $C(^3P_J)$ + C_2H_4 → C_3H_3 + H reaction dynamics between 0.49 and 30.8 kJ mol^{-1}. J Chem Phys 119:10607–10617

Gimondi I, Cavallotti C, Vanuzzo G, Balucani N, Casavecchia P (2016) Reaction dynamics of $O(^3P)$ + propyne: II. Primary products, branching ratios, and role of intersystem crossing from ab initio coupled triplet/singlet potential energy surfaces and statistical calculations. J Phys Chem A 120:4619–4633

Hänni N, Altwegg K, Balsiger H, Combi M, Fuselier SA, De Keyser J, Pestoni B, Rubin M, Wampfler SF (2021) Cyanogen, cyanoacetylene, and acetonitrile in comet 67P and their relation to the cyano radical. Astron Astrophys 647:A22

Herschbach DR (1987) Molecular dynamics of elementary chemical reactions (Nobel lecture). Angew Chem Int Ed 26:1221–1243

Hore NR, Russell DK (1998) Radical pathways in the thermal decomposition of pyridine and diazines: a laser pyrolysis and semiempirical study. J Chem Soc Perkin Trans 2:269–276

Jaber Al-Edhari A, Ceccarelli C, Kahane C, Viti S, Balucani N, Caux E, Faure A, Lefloch B, Lique F, Mendoza E et al (2017) History

of the solar-type protostar IRAS 16293–2422 as told by the cyanopolyynes. Astron Astrophys 597:A40

Laganà A, Garcia E, Paladini A, Casavecchia P, Balucani N (2012) The last mile of molecular reaction dynamics virtual experiments: the case of the OH(N=1–10) + CO(j=0–3) reaction. Faraday Discuss 157:415–436

Lee YT (1987a) Molecular beam studies of elementary chemical processes (Nobel Lecture). Science 236:793–798

Lee YT (1987b) Reactive scattering I: nonoptical methods. In: Scoles G (ed) Atomic and molecular beam methods, vol 1. Oxford University Press, New York, pp 553–568

Lee SH, Chen WK, Huang WJ (2009) Exploring the dynamics of reactions of oxygen atoms in states ^{3}P and ^{1}D with ethene at collision energy 3 kcal mol^{-1}. J Chem Phys 130:054301

Leonori F, Petrucci R, Segoloni E, Bergeat A, Hickson KM, Balucani N, Casavecchia P (2008) Unraveling the dynamics of the C(^{3}P,^{1}D) + C_2H_2 reactions by the crossed molecular beam scattering technique. J Phys Chem A 112:1363–1379 **(and refs. therein)**.

Leonori F, Petrucci R, Balucani N, Casavecchia P, Rosi M, Skouteris D, Berteloite C, Le Picard SD, Canosa A, Sims IR (2009) Crossed-beam dynamics, low temperature kinetics and theoretical studies of the reaction S(^{1}D) + C_2H_4. J Phys Chem A 113:15328–15345

Leonori F, Hickson KM, Le Picard SD, Wang XG, Petrucci R, Foggi P, Balucani N, Casavecchia P (2010) Crossed-beam universal-detection reactive scattering of radical beams characterized by laser-induced fluorescence: the case of C2 and CN. Mol Phys 108:1097–1113

Leonori F, Occhiogrosso A, Balucani N, Bucci A, Petrucci R, Casavecchia P (2012a) Crossed molecular beam dynamics studies of the O(^{3}P) + allene reaction: primary products, branching ratios, and dominant role of intersystem crossing. J Phys Chem Lett 3:75–80

Leonori F, Petrucci R, Wang X, Casavecchia P, Balucani N (2012b) A crossed beam study of the reaction CN+C_2H_4 at high collision energy: the opening of a new reaction channel. Chem Phys Lett 553:1–5

Leonori F, Balucani N, Capozza G, Segoloni E, Volpi GG, Casavecchia P (2014) Dynamics of the O(^{3}P) + C_2H_2 reaction from crossed molecular beam experiments with soft electron ionization detection. Phys Chem Chem Phys 16:10008–10022

Leonori F, Balucani N, Nevrly V, Bergeat A, Falcinelli S, Vanuzzo G, Casavecchia P, Cavallotti C (2015) Experimental and theoretical studies on the dynamics of the O(^{3}P) + propene reaction: primary products, branching ratios, and role of intersystem crossing. J Phys Chem C 119:14632–14652

Levine RD, Bernstein RB (1987) Molecular reaction dynamics and chemical reactivity. Oxford University Press, New York

Liang P, Mancini L, Marchione D, Vanuzzo G, Ferlin F, Recio P, Tan Y, Pannacci G, Vaccaro L, Rosi M, Casavecchia P, Balucani N (2022) Combined crossed molecular beams and computational study on the N(^{2}D) + HCCCN($X^1\Sigma^+$) reaction and implications for extra-terrestrial environments. Mol Phys 120:e1948126

Liang P, de Aragão EVF, Giani L, Mancini L, Pannacci G, Marchione D, Vanuzzo G, Faginas-Lago N, Rosi M, Skouteris D, Casavecchia P, Balucani N (2023a) OH($^2\Pi$) + C_2H_4 reaction: a combined crossed molecular beam and theoretical study. J Phys Chem A 127:4609–4623

Liang P, de Aragão EVF, Pannacci G, Vanuzzo G, Marchione D, Recio P, Stranges D, Casavecchia P, Faginas Lago N, Mancini L, Rosi M, Balucani N (2023b) Crossed-beam and theoretical studies of the combustion and astrochemistry relevant O(^{3}P) + HCCCN($X^1\Sigma^+$) (cyanoacetylene) reaction. J Phys Chem A 127:685–703

Lifshitz A, Tamburu C, Suslensky A (1989) Isomerization and decomposition of pyrrole at elevated temperatures: studies with a single-pulse shock tube. J Phys Chem 93:5802–5808

Lindberg JE, Aalto S, Costagliola F, Pérez-Beaupuits JP, Monje R, Muller S (2011) A survey of HC_3N in extragalactic sources. Astron Astrophys 527:A150

Liu S, Xiao C, Wang T, Chen J, Yang T, Xu X, Zhang DH, Yang X (2012) The dynamics of the D_2+OH →HOD+D reaction: a combined theoretical and experimental study. Faraday Discuss 157:101–111

Mackie JC, Colket MB III, Nelson PF (1990) An experimental study of the release of nitrogen from coals pyrolyzed in fluidized-bed reactors. J Phys Chem 94:4099–4106

Mancini L, Vanuzzo G, Marchione D, Pannacci G, Liang P, Recio P, Rosi M, Skouteris D, Casavecchia P, Balucani N (2021) The reaction N(^{2}D) + CH_3CCH (methylacetylene): a combined crossed molecular beams and theoretical investigation and implications for the atmosphere of Titan. J Phys Chem A 125:8846–8859

Marchione D, Mancini L, Liang P, Vanuzzo G, Pirani F, Skouteris D, Rosi M, Casavecchia P, Balucani N (2022) Unsaturated dinitriles formation routes in extraterrestrial environments: a combined experimental and theoretical investigation of the reaction between cyano radicals and cyanoethene (C_2H_3CN). J Phys Chem A 126:3569–3582

Martens HR, Reisenfeld DB, Williams JD, Johnson RE, Smith HD (2008) Observations of molecular oxygen ions in Saturn's inner magnetosphere. Geophys Res Lett 35:L20103

McElroy D, Walsh C, Markwick AJ, Cordiner MA, Smith K, Millar TJ (2013) The UMIST database for astrochemistry 2012. Astron Astrophys 550:A36

McGuire BA (2022) Census of interstellar, circumstellar, extragalactic, protoplanetary disk, and exoplanetary molecules. Astrophys J Suppl Ser 259:30

Mumma MJ, Charnley SB (2011) The chemical composition of comets—emerging taxonomies and natal heritage. Annu Rev Astron Astrophys 49:471–524

Murray VJ, Recio P, Caracciolo A, Miossec C, Balucani N, Casavecchia P, Minton TK (2020) Oxidation and nitridation of vitreous carbon at high temperatures. Carbon 167:388–402

Osborn DL, Zou P, Johnsen H, Hayden CC, Taatjes CA, Knyazev VD, North SW, Peterka DS, Ahmed M, Leone SR (2008) The multiplexed chemical kinetic photoionization mass spectrometer: a new approach to isomer-resolved chemical kinetics. Rev Sci Instrum 79:104103

Pan H, Liu K, Caracciolo A, Casavecchia P (2017) Crossed beam polyatomic reaction dynamics: recent advances and new insights. Chem Soc Rev Ed 46:7517–7547

Pannacci G, Mancini L, Vanuzzo G, Liang P, Marchione D, Rosi M, Casavecchia P, Balucani N (2023) Combined crossed-beams and theoretical study of the O(^{3}P,^{1}D) + acrylonitrile (CH_2CHCN) reactions and implications for combustion and extraterrestrial environments. Phys Chem Chem Phys 25:20194–20211

Parker DSN, Kaiser RI, Kostko O, Troy TP, Ahmed M, Sun BJ, Chen SH, Chang AHH (2015) On the formation of pyridine in the interstellar medium. Phys Chem Chem Phys 17:32000–32008

Puzzarini C, Barone V (2020) A never-ending story in the sky: the secrets of chemical evolution. Phys Life Rev 32:59–94

Qiu M, Ren Z, Che L, Dai D, Harich SA, Wang X, Yang X, Xu C, Xie D, Gustafsson M, Skodje RT, Sun Z, Zhang DH (2006) Observation of Feshbach resonances in the F + H_2 → HF + H reaction. Science 311:1440–1443

Recio P, Marchione D, Caracciolo A, Murray V, Mancini L, Rosi M, Casavecchia P, Balucani N (2021) A crossed molecular beam

investigation of the N(2D) + pyridine reaction and implications for prebiotic chemistry. Chem Phys Lett 779:138852

Recio P, Alessandrini S, Vanuzzo G, Pannacci G, Baggioli A, Marchione D, Caracciolo A, Murray VJ, Casavecchia P, Balucani N, Cavallotti C, Puzzarini C, Barone V (2022) Intersystem crossing in the entrance channel of the reaction of O(^{3}P) with pyridine. Nat Chem 14:1405–1412

Ruscic B, Bross DH (2020) Active thermochemical tables (ATcT) values based on ver. 1.122o of the thermochemical network; available at ATcT.anl.gov

Ruscic B, Pinzon RE, Morton ML, von Laszewski G, Bittner S, Nijsure SG, Amin KA, Minkoff M, Wagner AF (2004) Introduction to active thermochemical tables: several "key" enthalpies of formation revisited. J Phys Chem A 108:9979–9997

Ruscic B, Pinzon RE, von Laszewski G, Kodeboyina D, Burcat A, Leahy D, Montoya D, Wagner AF (2005) Active thermochemical tables: thermochemistry for the 21st century. J Phys Conf Ser 16:561–570

Schmoltner AM, Chu PM, Lee YT (1989) Crossed molecular beam study of the reaction O(^{3}P) + C_2H_2. J Chem Phys 91:5365–5373

Schnieder S-R, Borkowski J, Wrede E, Welge KH, Aoiz FJ, Bañares L, D'Mello MJ, Herrero VJ, Saez Rabanos V, Wyatt RE (1995) Experimental studies and theoretical predictions for the H + D_2 → HD + D reaction. Science 269:207–210

Snyder LR (1969) Nitrogen and oxygen compound types in petroleum. Anal Chem 41:314–323

Strazisar BR, Lin C, Davis HF (2000) Mode-specific energy disposal in the four-atom reaction OH + D_2 → HOD + D. Science 290:958–961

Suzuki H, Yamamoto S, Ohishi M, Kaifu N, Ishikawa SI, Hirahara Y, Takano SJTAJ (1992) A survey of CCS, HC_3N, HC_5N, and NH_3 toward dark cloud cores and their production chemistry. Astrophys J 392:551–570

Szczepaniak U (2017) Spectroscopy and photochemistry of astrophysically-relevant molecules of the cyanoactylene family. Chemical Physics [physics.chem-ph]. Université Paris Saclay (COmUE); Instytut chemii fizycznej (Pologne). English. ffNNT: 2017SACLS128

Taatjes CA, Hansen N, Osborn DL, Kohse-Höinghaus K, Cool TA, Westmoreland PR (2008) '"Imaging"' combustion chemistry via multiplexed synchrotron-photoionization mass spectrometry. Phys Chem Chem Phys 10:20–34

Teanby NA, Irwin PGJ, de Kok R, Vinatier S, Bézard B, Nixon CA, Flasar FM, Calcutt SB, Bowles NE, Fletcher L, Howett C, Taylor FW (2007) Vertical profiles of HCN, HC_3N, and C_2H_2 in Titan's atmosphere derived from Cassini/CIRS data. Icarus 186:364–384

Tenenbaum ED, Apponi AJ, Ziurys LM (2006) Detection of C_3O in IRC+10216: oxygen-carbon chain chemistry in the outer envelope. Astrophys J 649:L17–L20

Terentis A, Doughty A, Mackie JC (1992) A kinetic study of the oxidation of pyridine. J Phys Chem 96:10334–10339

Turner BE (1971) Detection of interstellar cyanoacetylene. Astrophys J 163:L35–L39

van Dishoeck EF, Blake GA, Jansen DJ, Groesbeck TD (1995) Molecular abundances and low-mass star formation. II. Organic and deuterated species toward IRAS 16293–2422. Astrophys J 447:760–782

Vanuzzo G, Balucani N, Leonori F, Stranges D, Falcinelli S, Bergeat A, Casavecchia P, Gimondi I, Cavallotti C (2016a) Isomer-specific chemistry in the propyne and allene reactions with oxygen atoms: CH_3CH + CO versus CH_2CH_2 + CO products. J Phys Chem Lett 7:1010–1015

Vanuzzo G, Balucani N, Leonori F, Stranges D, Nevrly V, Falcinelli S, Bergeat A, Casavecchia P, Cavallotti C (2016b) Reaction dynamics of O(^{3}P) + propyne: I. Primary products, branching ratios, and role of intersystem crossing from crossed molecular beam experiments. J Phys Chem A 120:4603–4618

Vanuzzo G, Caracciolo A, Minton TK, Balucani N, Casavecchia P, de Falco C, Baggioli A, Cavallotti C (2021) Crossed-beams and theoretical studies of the O(^{3}P,^{1}D) + benzene reactions: primary products, branching fractions, and role of intersystem crossing. J Phys Chem A 125:8434–8453

Vanuzzo G, Marchione D, Mancini L, Liang P, Pannacci G, Recio P, Tan Y, Rosi M, Skouteris D, Casavecchia P, Balucani N (2022a) The N(^{2}D) + CH_2CHCN (vinyl cyanide) reaction: a combined crossed molecular beam and theoretical study and implications for the atmosphere of Titan. J Phys Chem A 126:6110–6123

Vanuzzo G, Mancini L, Pannacci G, Liang P, Marchione D, Recio P, Tan Y, Rosi M, Skouteris D, Casavecchia P, Balucani N, Hickson KM, Loison JC, Dobrijevic M (2022b) Reaction N(^{2}D) + CH_2CCH_2 (Allene): an experimental and theoretical investigation and implications for the photochemical models of Titan. ACS Earth Space Sci 6:2305–2321

Vanuzzo G, Caracciolo A, Yuan D, Mancini L, Skouteris D, Rosi M, Casavecchia P, Balucani N (2024) Crossed beam and theoretical studies of the Titan relevant N(^{2}D) + toluene reactions: primary products and branching fractions. J Phys Chem A **(in preparation)**

Wakelam V, Herbst E, Loison JC, Smith IWM, Chandrasekaran V, Pavone B, Adams NG, Bacchus-Montabone MC, Bergeat A, B´eroff K, et al (2012) A kinetic database for astrochemistry (KIDA). Astrophys J Suppl Ser 199:21

Wallace S, Bartle KD, Perry DL (1989) Quantification of nitrogen functional groups in coal and coal derived products. Fuel 68:1450–1455

Walmsley CM, Güsten R, Angerhofer P, Churchwell E, Mundy L (1986) Cyanoacetylene in the Sgr A molecular clouds. Astron Astrophys 155:129–136

Wang X, Dong W, Xiao C, Ren Z, Dai D, Wang X, Casavecchia P, Yang X, Jiang B, Xie D, Zhang DH, Werner HJ, Alexander MH (2008) The extent of non-Born-Oppenheimer coupling in the reaction of Cl(^2P) with *para*-H_2. Science 322:573–576

Wang BB, Sun LS, Su S, Xiang J, Hu S, Fei H (2012) A kinetic study of NO formation during oxy-fuel combustion of pyridine. Appl Energy 92:361–368

Woodall J, Agúndez M, Markwick-Kemper AJ, Millar TJ (2007) UMIST DATABASE for Astrochemistry 2006.Astron Astrophys 466:1197–1204

Xie HB, Ding YH, Sun CC (2006) Reaction mechanism of oxygen atoms with cyanoacetylene in the gas phase and on water ice. Astrophys J 643:573–581

Yang X, Lin J, Lee YT, Blank DA, Suits AG, Wodtke AM (1997) Universal crossed molecular beams apparatus with synchrotron photoionization mass spectrometric product detection. Rev Sci Instrum 68:3317–3326

Yuan D, Yu S, Chen W, Sang J, Luo C, Wang T, Xu X, Casavecchia P, Wang X, Sun Z, Zhang DH, Yang X (2018) Direct observation of forward-scattering oscillations in the H+HD→H_2+D reaction. Nat Chem 10:653–658

Zhang XY, Zhu QF, Li J, Chen X, Wang JZ, Zhang JS (2017) A spectral line survey of IRC+10216 between 13.3 and 18.5 GHz. Astron Astrophys 606:A74